Cell Reports

Article

Stress-dependent inhibition of polarized cell growth through unbalancing the GEF/GAP regulation of Cdc42

Graphical abstract

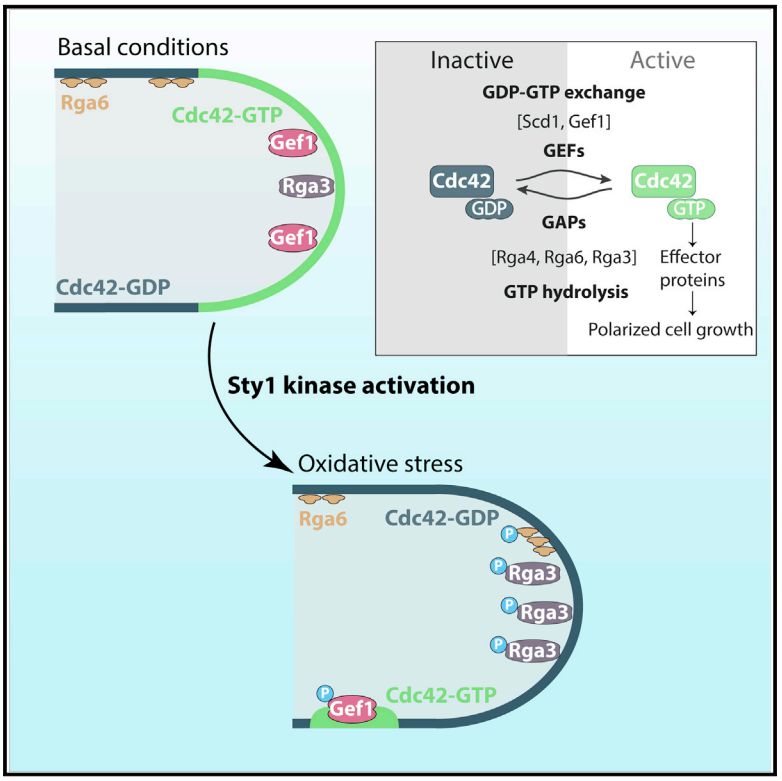

Highlights

- Oxidative stress causes Sty1-kinase-dependent inactivation of Cdc42 at cell poles
- The GAPs Rga3/6 and the GEF Gef1 are direct targets of Sty1 kinase
- Increased GAP activity at the cell poles mediates Cdc42 depolarization upon stress
- Gef1 delocalization from cell tips promotes stress-dependent Cdc42 inactivation

Authors

Clàudia Salat-Canela, Mercè Carmona, Rebeca Martín-García, Pilar Pérez, José Ayté, Elena Hidalgo

Correspondence

piper@usal.es (P.P.), jose.ayte@upf.edu (J.A.), elena.hidalgo@upf.edu (E.H.)

In brief

MAP kinases allow eukaryotic organisms to cope with environmental challenges. The fission yeast MAP kinase Sty1 couples stress signals with the Cdc42 polarity module, leading to the inhibition of polarized cell growth. Salat-Canela et al. decipher the molecular mechanism downstream of Sty1 that mediates the Cdc42 depolarization response.

Salat-Canela et al., 2021, Cell Reports 37, 109951
November 2, 2021
https://doi.org/10.1016/j.celrep.2021.109951

CellPress

Cell Reports

CellPress
OPEN ACCESS

Article

Stress-dependent inhibition of polarized cell growth through unbalancing the GEF/GAP regulation of Cdc42

Clàudia Salat-Canela,[1] Mercè Carmona,[1] Rebeca Martín-García,[2] Pilar Pérez,[2,*] José Ayté,[1,*] and Elena Hidalgo[1,3,*]
[1]Oxidative Stress and Cell Cycle Group, Universitat Pompeu Fabra, C/ Dr. Aiguader 88, 08003 Barcelona, Spain
[2]Instituto de Biología Funcional y Genómica (IBFG), Consejo Superior de Investigaciones Científicas, Universidad de Salamanca, 37007 Salamanca, Spain
[3]Lead contact
*Correspondence: piper@usal.es (P.P.), jose.ayte@upf.edu (J.A.), elena.hidalgo@upf.edu (E.H.)
https://doi.org/10.1016/j.celrep.2021.109951

SUMMARY

Cdc42 GTPase rules cell polarity and growth in fission yeast. It is negatively and positively regulated by GTPase-activating proteins (GAPs) and guanine nucleotide exchange factors (GEFs), respectively. Active Cdc42-GTP localizes to the poles, where it associates with numerous proteins constituting the polarity module. However, little is known about its downregulation. We describe here that oxidative stress causes Sty1-kinase-dependent Cdc42 inactivation at cell poles. Both the amount of active Cdc42 at tips and cell length inversely correlate with Sty1 activity, explaining the elongated morphology of *Δsty1* cells. We have created stress-blinded cell poles either by eliminating two Cdc42 GAPs or through the constitutive tethering of Gef1 to cell tips, and we biochemically demonstrate that the GAPs Rga3/6 and the GEF Gef1 are direct substrates of Sty1. We propose that phosphorylation of Rga3/6 and Gef1 mediates the Sty1-dependent inhibition of Cdc42 at cell tips, halting polarized growth during stress adaptation.

INTRODUCTION

Ras-homologous (Rho) GTPases regulate cell polarity and growth in eukaryotes. In particular, Cdc42 has a central role in the establishment of polarized growth. In budding yeast, Cdc42 localizes exclusively at the site of bud growth during division, but this model system cannot be used to explain multiple growing areas existing in other cell types, including fission yeast. *Schizosaccharomyces pombe* cells display not only Cdc42 activity sites at the area of cell division but also monopolar Cdc42-dependent growth from the old end just after cell division, and they shift to a bipolar mode when reaching a certain length in a process known as NETO (new-end takeoff) (Mitchison and Nurse, 1985). Therefore, *S. pombe* is an excellent model to study multiple polarity sites. Furthermore, wild-type cells have a rod-like phenotype, while decreased Cdc42 levels lead to a rounded phenotype (Miller and Johnson, 1994).

Cdc42 localization and activation are tightly regulated in space and in time. Cdc42 acts as a switch that can be found in a GTP- or a GDP-bound state, and this modulates its ability to interact with other components. Therefore, different GEFs (guanine nucleotide exchange factors) activate Cdc42, and GAPs (GTPase-activating proteins) negatively regulate its activity. Additionally, *S. pombe* Cdc42 local activation promotes its accumulation at the growth regions of the plasma membrane (Bendezú et al., 2015; Estravís et al., 2017). Two GEFs have been characterized for Cdc42: Scd1, which localizes at cell tips with Cdc42-GTP during interphase (Kelly and Nurse, 2011), and Gef1, with apparent cytoplasmic localization (Tay et al., 2018). Both GEFs are found at the cytokinetic ring during cell division (Coll et al., 2003; Hirota et al., 2003). Regarding GAPs, Rga4 was described early; it localizes to the cell sides (Das et al., 2007; Tatebe et al., 2008). Rga6 has similar lateral localization, and it has been proposed to collaborate with Rga4 to spatially restrict active Cdc42 to the cell tips (Revilla-Guarinos et al., 2016). Rga3 has been recently described as a Cdc42 GAP localized to the cell tips. Its absence does not lead to any detectable phenotype during mitotic cell growth. Instead, Rga3 does play a role during sexual reproduction by regulating Cdc42 activity at the polarity patch (Gallo Castro and Martin, 2018).

How are new polarity sites established at a given position? In both *Saccharomyces cerevisiae* and *S. pombe*, the formation of a quaternary complex between Cdc42, a p21-activated kinase (PAK1/CLA4 or Pak1), a scaffolding protein (BEM1 or Scd2), and the GEF (CDC24 or Scd1) is crucial to enhance local activation of Cdc42. The recruitment of the GEF for Cdc42-GTP at the membrane favors the activation of neighboring Cdc42 molecules, creating a positive feedback loop that contributes to the creation of new polarity sites (for a review, see Chiou et al., 2017). In fission yeast, the distinct spatial distribution of GEFs and GAPs is also vital to seed sites of polarity. Therefore, the landmark established by Tea1 and Tea4, driven to the cell tips by microtubules, promotes local activation of Cdc42 at cell tips by excluding Rga4 (Kokkoris et al., 2014).

While positive feedback loops probably explain the concentration in space and time of the Cdc42 module at one particular position (for review, see Chiou et al., 2017; Martin, 2015), negative regulators of active Cdc42 are required to explain the oscillatory behavior of the module in post-NETO bipolar fission yeast cells (Das et al., 2012) and limit the spreading of the polarity cluster. A relevant example of the later is the inhibitory phosphorylation of *S. cerevisiae* CDC24, the main GEF of CDC42, by its downstream effector PAK, to downregulate the polarity sites as a negative feedback loop (Gulli et al., 2000; Kuo et al., 2014; Rapali et al., 2017; Wai et al., 2009).

Stress signals mediated by the mitogen-activated protein (MAP) kinase Sty1 pathway in fission yeast cause dispersion of the Cdc42 polarity module (Mutavchiev et al., 2016). Thus, latrunculin A (LatA)-activated Sty1 promotes Cdc42-GTP dispersal from cell tips. In response to environmental stresses, Sty1 is phosphorylated and triggers a core environmental stress response, mainly based on the transcription factor Atf1. Stress-dependent phosphorylation of the MAP kinase, which is kept inactive in the absence of stress by several phosphatases such as Pyp1 (Millar et al., 1995; Shiozaki and Russell, 1995b), triggers its nuclear accumulation and the phosphorylation of Atf1 (Salat-Canela et al., 2017; Wilkinson et al., 1996). Cells lacking Sty1 show reduced tolerance to many environmental stresses such as heat shock, oxidative stress, and nutritional deprivation (Toone et al., 1998; Zuin et al., 2010). *Δsty1* cells display an elongated "*cdc*"-like phenotype, suggesting that Sty1 may also have a role at the G2/M transition (Shiozaki and Russell, 1995a).

Here, we investigated whether environmental stress regulating the Sty1 pathway could modulate the activity of Cdc42 at the growth area and whether this regulation could explain the elongated phenotype of *Δsty1* cells. We show here that hydrogen peroxide (H_2O_2), which transiently activates Sty1, also triggers active Cdc42 dispersal from the cell tips in a Sty1-dependent manner without promoting actin depolymerization and that stress-independent Sty1 activation is sufficient to induce these effects on polarity. We demonstrate that Sty1 activity inversely correlates with active Cdc42 at cell tips and, importantly, with cell length. Furthermore, Sty1's inhibitory role in Cdc42 activity may be exerted through activation at cell tips of Rga3 and Rga6 GAPs and the combined Gef1 delocalization and inactivation of Scd1, with a net transient inhibition of Cdc42 and polarized growth cessation. Indeed, we demonstrate that Rga3 and Gef1 are direct targets of active Sty1.

RESULTS

H_2O_2 triggers a Sty1-dependent and actin depolymerization-independent inactivation of Cdc42 at cell tips

In the presence of the actin depolymerization drug LatA, the active Cdc42 polarity module is dispersed from cell tips in a Sty1-dependent manner (Mutavchiev et al., 2016). Sty1 is strongly activated by H_2O_2 to trigger a gene expression program (Chen et al., 2003). We used GFP-tagged CRIB (Cdc42/Rac interactive binding motif) to monitor active GTP-bound Cdc42 in the presence of H_2O_2 (Ozbudak et al., 2005; Tatebe et al., 2008). As shown in Figure 1A, treatment of wild-type cells with either LatA or H_2O_2 causes dispersal of active Cdc42 from the cell tips to lateral patches (indicated with arrows). The loss of CRIB-GFP at cell poles follows similar kinetics upon LatA and H_2O_2 treatments (Figure 1B). We used Lifeact-mCherry as a marker to label F-actin in living cells (Huang et al., 2012). As reported before (Mutavchiev et al., 2016), actin depolymerization upon LatA imposition is faster than CRIB-3GFP dispersal from tips (Figure 1A). H_2O_2 treatment does not significantly perturb the actin cytoskeleton (Figure 1A) and nevertheless causes CRIB-3GFP dispersal. Both types of treatments (the irreversible inhibitor LatA and the transient natural stressor H_2O_2) cause a permanent or temporal growth inhibition (respectively), as demonstrated by growth curves (Figure S1A) and measuring net cell elongation rates after stress imposition in time-lapse experiments (Figures 1C and S1B). In conclusion, oxidative stress causes inactivation of the polarity module at cell tips, which is concomitant to cell growth cessation.

Stress-dependent positioning of the Cdc42 polarity module to lateral patches is dependent on the Cdc42 GEF Gef1

Stress imposition causes CRIB dispersal from the tips to lateral patches upon H_2O_2 (see arrows in Figure 1A) or LatA treatments (Bendezú and Martin, 2011; Mutavchiev et al., 2016). We tested the presence of different Cdc42 module components at both cell sites before and after stress imposition. As shown in Figure 2A, the main Cdc42 GEF Scd1 and its scaffold, Scd2, are localized to cell tips prior to stress and are totally (Scd1-GFP) or partially (Scd2-GFP) dispersed from the poles upon peroxide treatment. The downstream effector kinase Pak1 is also dispersed from the poles after stress imposition, probably as a consequence of Cdc42 inactivation (Figure 2A). Upon exit from the cell tips, Scd2 and Pak1, but not Scd1, are present at the lateral patches of active Cdc42 (see white arrows in Figure 2A), suggesting that a GEF other than Scd1 is responsible for the active Cdc42 present at lateral surfaces, which appear after stress imposition. In fact, the Scd1 scaffold Scd2 is not required for the formation of the active Cdc42 patches (Figure S2A). Gef1-3YFP is located at the cytosol but also decorates the tips of non-dividing cells prior to stress; the localization at tips is lost upon H_2O_2 stress, with Gef1-3YFP clearly localizing to lateral patches 45 min after stress imposition (see white arrow in Figure 2B). Indeed, while dispersal of CRIB-3GFP from cell tips upon H_2O_2 (Figure 2C) or LatA (Figure S2B) treatment is not blocked in strain *Δgef1*, the formation of the lateral patches is completely dependent on the presence of Gef1 (Figures 2C and S2B), as shown using other stressors (Chen et al., 2019; Hercyk et al., 2019). We conclude that stress promotes redistribution of the active Cdc42 polarity module from the cell tips toward side patches, which contain and require Gef1, but not Scd1 (Figure 2D). We will use hereafter these lateral sites as a secondary hallmark of stress-dependent cell growth arrest.

Active Sty1 directly promotes the inactivation of Cdc42 at cell tips

To confirm that active Sty1 directly drives the redistribution of the Cdc42-dependent polarity module from the poles to the sides of the cell, we pursued three types of strategies: (1) we first tested the effect of H_2O_2 in CRIB-3GFP dispersal in cells lacking Sty1,

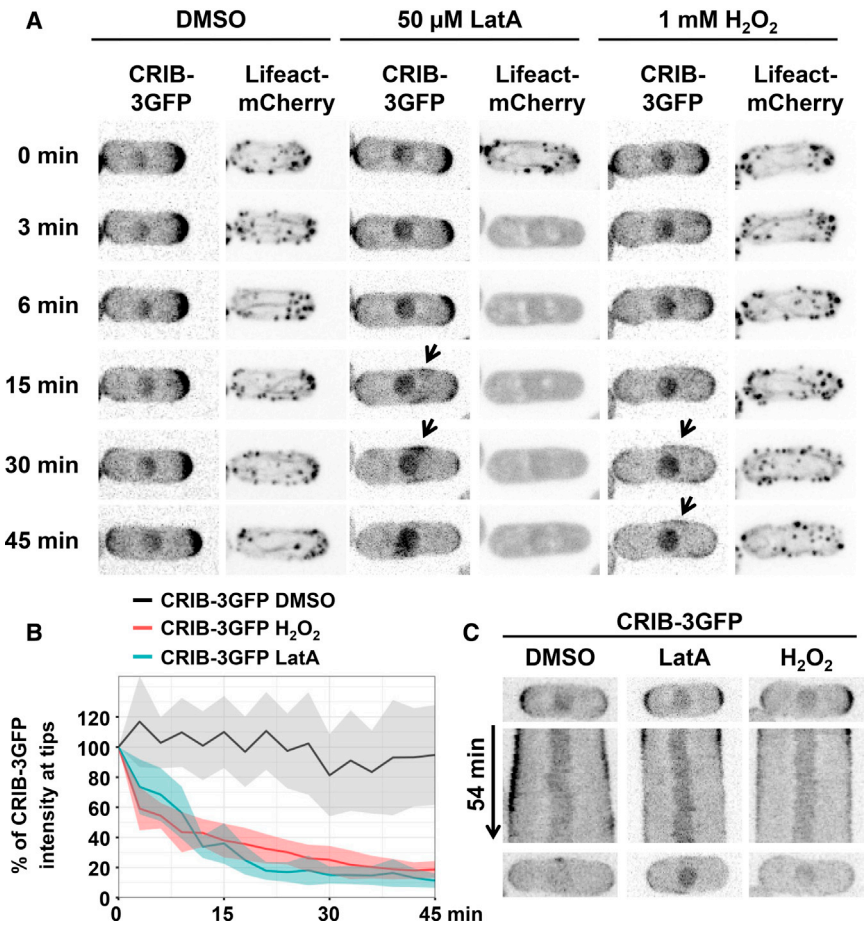

Figure 1. Activation of the Sty1 MAP kinase by oxidative stress leads to Cdc42 depolarization from cell tips

(A) CRIB dispersal from cell tips after oxidative stress imposition follows similar kinetics than in LatA treatment. Images depicting GTP-bound Cdc42 and F-actin at several points from time-lapse experiments in YE cultures of CS208 (expressing CRIB-3GFP and Lifeact-mCherry) during DMSO, 1 mM H_2O_2, or 50 μM LatA treatments. Arrows point to the formation of Cdc42-GTP lateral patches.

(B) Quantification of CRIB-3GFP intensity at cell tips in time-lapse experiments as described in (A). Data are represented as a percentage with respect to time zero. The shaded area represents SD. At least nine cells were analyzed for each condition from three independent biological replicates.

(C) Cell growth ceases after treatment with LatA or H_2O_2. Kymographs showing CRIB-3GFP cells from time-lapse experiments as shown in (A).

See also Figure S1.

(2) we analyzed whether the downstream transcription factor Atf1 is required to trigger H_2O_2-dependent cellular depolarization, and (3) we used genetically engineered cells expressing a stress-independent active Sty1 allele to study the effect of this Sty1 on Cdc42 activity.

We expressed CRIB-tdTomato (Revilla-Guarinos et al., 2016) in wild-type and *Δsty1* cells overexpressing catalase to minimize the direct toxic effect of intracellular peroxides in cells lacking the MAP kinase. Overexpression of catalase in wild-type cells does not alter the inhibitory effect of stress on active Cdc42 at cell tips (Figures 3A and S3A). Active Cdc42 is not redistributed from cell poles to cell sides upon H_2O_2 addition in cells lacking Sty1 (Figures 3A and 3B), and polarized growth is not inhibited in these cells (Figures 3C and S3B). Second, the absence of Atf1, required to trigger the transcriptional response (Chen et al., 2003, 2008), does not largely affect CRIB-3GFP dispersal from cell tips upon stress imposition (Figures S3C and S3D), which suggests that Sty1 kinase activity is itself required at cell tips.

In a third strategy, we monitored CRIB-3GFP in cells expressing the analog-sensitive mutant Sty1.AS from the endogenous *sty1* locus (Gregan et al., 2007; Zuin et al., 2010) and lacking Pyp1, the main Sty1 phosphatase (Millar et al., 1995; Shiozaki and Russell, 1995a) (Figure 3D). In the Sty1.AS protein, the T97A mutation in the kinase ATP pocket facilitates the entry of the bulky inhibitory ATP analog 3MB-PP1, which fully blocks H_2O_2-dependent Sty1.AS activity without affecting wild-type Sty1 (Figures 3E and S3E). Cells lacking Pyp1 display basal activation of Sty1 under unstressed conditions (Shiozaki and Russell, 1995a), but addition of 3MB-PP1 keeps Sty1.AS inactive and downstream Atf1 dephosphorylated, until the analog is withdrawn (Figure 3E). In the presence of the kinase inhibitor, CRIB-3GFP expressed in *Δpyp1 sty1.AS* cells localizes to cell tips, but removal of the analog quickly triggers CRIB dispersal from the poles (Figure 3F), with kinetics similar to the effect of H_2O_2 addition to CRIB-3GFP-expressing wild-type cells (compare Figure S3F and Figure 1B). We conclude that direct activation of the Sty1 kinase, either genetically or upon stress imposition, is sufficient to redistribute the Cdc42 polarity module away from the cell tips.

Cell length and activity of Cdc42 at the tips inversely correlate to Sty1 activity

The rod-shaped morphology and tip elongation growth of fission yeast has enabled the isolation of mutations advancing or delaying cell-cycle progression based on cell length at division. In fact, a genetic interaction was described more than two decades ago between Sty1 and the cell-cycle machinery (Shiozaki and Russell, 1995a). We have measured cell length and CRIB intensity (as a measure of active Cdc42 levels) at cell poles of different MAP kinase pathway mutants before cell division (Figures 4A–4C). While *Δsty1* cells are longer than wild-type cells, *Δpyp1* cells (in which the Sty1 pathway is constitutively activated) are shorter (Figures 4A and 4B). Importantly, CRIB-3GFP expression does not affect cell size in the different backgrounds (compare Figures 4A and 4B with Figure S4A). It is worth noting that *Δatf1* cells are

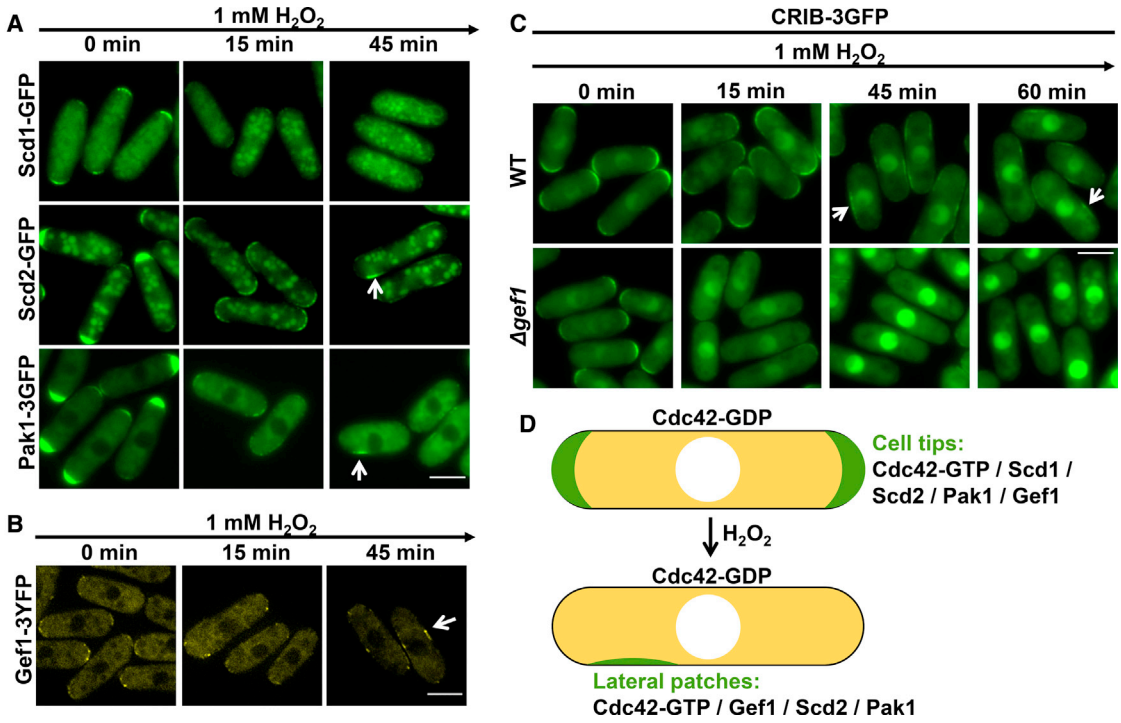

Figure 2. Formation of active Cdc42 lateral patches is dependent on Gef1

(A) Scd2 and Pak1 proteins are localized at Cdc42-GTP lateral patches after stress imposition. Images from logarithmic YE cultures of PPG56.66 (Scd1-GFP), PPG142.42 (Scd2-GFP), and PPG69.03 (Pak1-GFP), treated or not with 1 mM H_2O_2. White arrows point to lateral patches.

(B) Gef1 is the unique GEF detected at lateral patches. Images from logarithmic YE cultures of FV1218 (Gef1-3YFP), treated or not with 1 mM H_2O_2. White arrows point to lateral patches.

(C) Activation of Cdc42 at cortical regions exclusively depends on Gef1. Images of GTP-bound Cdc42 from logarithmic YE cultures of PPG65.60 (wild-type strain expressing CRIB-3GFP) and PPG70.07 (*Δgef1* strain expressing CRIB-3GFP), treated or not with 1 mM H_2O_2. Arrowheads point to the presence of Cdc42-GTP at lateral patches.

(D) Scheme depicting the localization of several Cdc42 polarity module components before and after stress imposition.

Scale bar, 5 μm. See also Figure S2.

similar in size to wild type, confirming our previous observation that the effect of Sty1 in Cdc42 regulation is independent of transcription (Figure 4B). Regarding the levels of active Cdc42 (CRIB-3GFP) at cell tips (Figure 4C), we determined a 2-fold increase in CRIB-3GFP fluorescence intensity in *Δsty1* cells; in contrast, we detected a significant decrease of active Cdc42 at the tips of *Δpyp1* cells, enforcing the idea that Sty1 activity is required to control Cdc42 at cell tips also under unstressed conditions. We did not observe enhanced CRIB levels in cell-cycle mutants with elongated phenotypes, such as *cdc25-22* (data not shown), suggesting that cell size per se does not control active Cdc42 at cell tips.

A consequence of active Cdc42 deposition at cell tips may be an increase in the growth rate. We measured cellular growth rates of wild-type, *Δsty1*, *Δatf1*, and *Δpyp1* strains by incubating cultures with fluorescein isothiocyanate (FITC)-lectin, which stains cell surface carbohydrates in green; the dye was washed out, and growth proceeded for 90 min to expose unlabeled growth areas, which were counterstained with calcofluor (visualized in red) to highlight new growth surfaces (see STAR Methods for details) (Figure S4B). In order to compare strains pairwise, we labeled wild-type cells with a nuclear fluorescent reporter, Hta1-mRFP. This tag did not affect the growth rate of wild-type cells (Figure 4D, left panel). While wild-type cells (labeled with Hta1-mRFP) elongated at a rate of ~3 μm/h, *Δsty1* cells did it much faster (≥4 μm/h), and *Δpyp1* cells elongated slower (≤2 μm/h) (Figure 4D). As expected, *Δatf1* cells grew at the same rate as wild-type cells.

To completely separate cytosolic from nuclear Sty1 activity, we generated a Sty1 chimera fused to the Tea1 polarity marker, which localizes to cell tips (Mata and Nurse, 1997). This Tea1-Sty1-GFP chimera localized at cell tips in a wild-type or *Δsty1* background (Figure 4E). We also confirmed that this chimera is unable to activate the transcriptional cascade downstream of Sty1 using two different approaches: (1) in the absence of endogenous Sty1, Atf1 was not phosphorylated upon H_2O_2 treatment, indicating that the chimera lacks Sty1 nuclear functions (Figure S4C); (2) *Δsty1* cells expressing Tea1-Sty1-GFP are as sensitive to H_2O_2 in liquid growth as cells lacking Sty1 (Figure S4D). Altogether, these results demonstrate than Tea1-Sty1-GFP lacks nuclear functions. We then tested whether the chimera, which is constitutively trapped at cell tips, contributed to regulate cell length at septation. As can be observed in Figure 4F, expressing Tea1-Sty1-GFP slightly, but significantly,

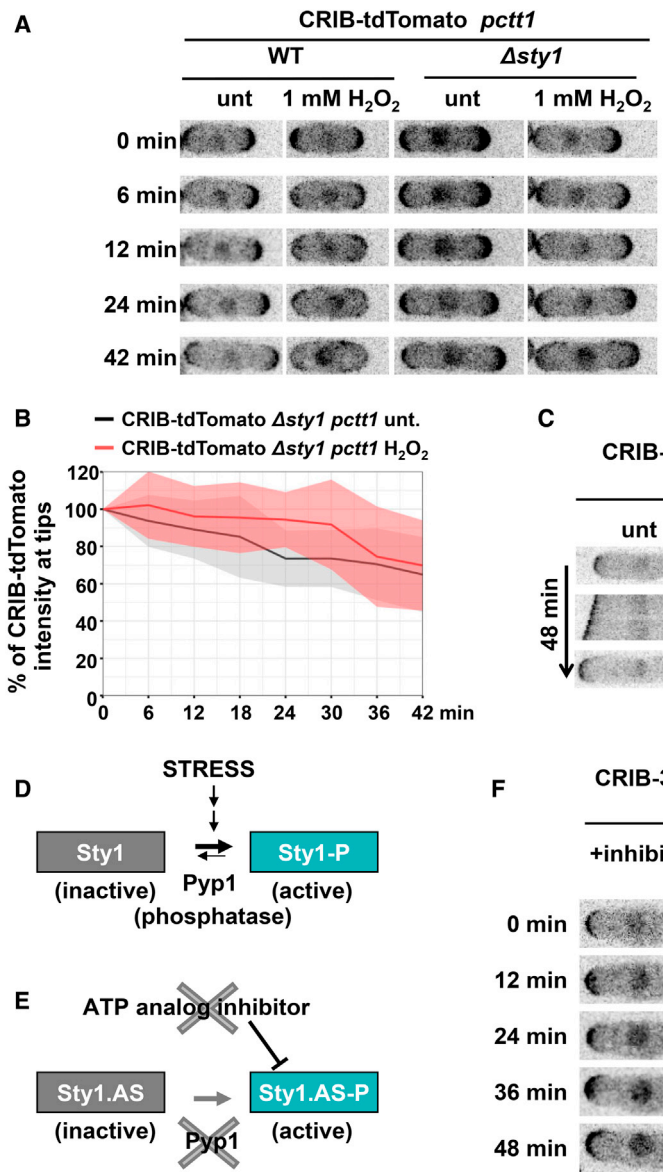

Figure 3. Cdc42 depolarization from cell tips after oxidative stress depends on Sty1 activity

(A) CRIB signal is not dispersed form cell tips upon H_2O_2 treatment in *Δsty1* cells. Images of GTP-bound Cdc42 from time-lapse experiments of YE cultures of CS245 (wild-type cells expressing CRIB-tdTomato and Ctt1) and CS238 (*Δsty1* cells expressing CRIB-tdTomato and Ctt1) untreated (unt) or treated with 1 mM H_2O_2.

(B) Quantification of CRIB-tdTomato signal at cell tips in time-lapse experiments as described in (A). Data representation was done as in Figure 1B.

(C) Cell growth is not halted in *Δsty1* cells after stress imposition. Kymographs showing CRIB-tdTomato cells from time-lapse experiments as described in (A).

(D and E) Schematic representation of the *sty1.AS Δpyp1* strain. In wild-type cells, Sty1 activation is counteracted by the phosphatase Pyp1, eventually leading to the shutoff of the cascade. In the *sty1.AS Δpyp1* mutant, Sty1 can be artificially activated by removing the ATP analog.

(F) Stress-independent activation of Sty1 leads to Cdc42-GTP dispersal from cell tips. Images of GTP-bound Cdc42 staining from YE cultures of CS147 (*sty1.AS Δpyp1* expressing CRIB-3GFP) in the presence of or after the removal of 10 μM of the inhibitor 3MB-PP1.

See also Figure S3.

reduced cell length at division in wild-type cells. More noticeably was the effect in a *Δsty1* background, where expressing Tea1-Sty1-GFP reduced the length at septation from ≥20 μm to ~15 μm (Figure 4F); importantly, CRIB levels in *Δsty1* cells were also reduced by expression of Tea1-Sty1 (Figure S4E). We propose that Sty1 activity inversely correlates with Cdc42 activity at cell tips (Figure 4G).

Cells devoid of the Cdc42 GAPs Rga3 and Rga6 are insensitive to stress-dependent cell polarity inhibition

In the search for downstream effectors of Sty1 in the polarity module, we first interrogated the putative GAPs of Cdc42. Rga4 and Rga6 localize to cell sides and contribute to the spatial restriction of active Cdc42 at cell poles (Revilla-Guarinos et al., 2016; Tatebe et al., 2008), while Rga3 co-exists with Cdc42-GTP at growth sites (Gallo Castro and Martin, 2018). We first monitored the localization of Rga3, Rga4, and Rga6 after environmental stress. We co-expressed CRIB-3mCherry and GFP-tagged versions of each GAP. While a weak signal of Rga3-GFP can be detected at cell tips during unstressed conditions, the green fluorescence of the GFP protein is significantly increased after treatment with H_2O_2, inversely correlating with the CRIB-3mCherry fluorescence (Figures 5A and 5B). Rga4-GFP remains in lateral patches before and after stress imposition (Figure 5C), and *Δrga4* cells are sensitive to CRIB-GFP tip depolarization after H_2O_2 stress (Figure S5A), discarding any role of this GAP in Sty1-dependent Cdc42 inhibition. After H_2O_2 imposition, Rga6-GFP still localizes at the lateral membranes but it is also present at the cell tips (Figure 5C), as reported before upon LatA treatment (Figure S5B) (Revilla-Guarinos et al., 2016). Moreover, in *Δsty1* cells, Rga6-GFP is excluded from cell tips even after LatA treatment (Figure S5B), indicating that Rga6 localization may be somehow regulated by Sty1. Therefore, two GAPs are present at cell tips after stress (Rga3 and Rga6) and are candidates to trigger Cdc42 inactivation (Figure 5D).

We then tested the effect of single and double deletions of GAP-coding genes on stress-dependent inactivation of cell polarity. Cells lacking Rga3 retain active Cdc42-GTP at cell tips 60 min after H_2O_2 imposition (Figures 5E and 5F), while *Δrga6* cells display H_2O_2 inactivation kinetics similar to wild-type cells

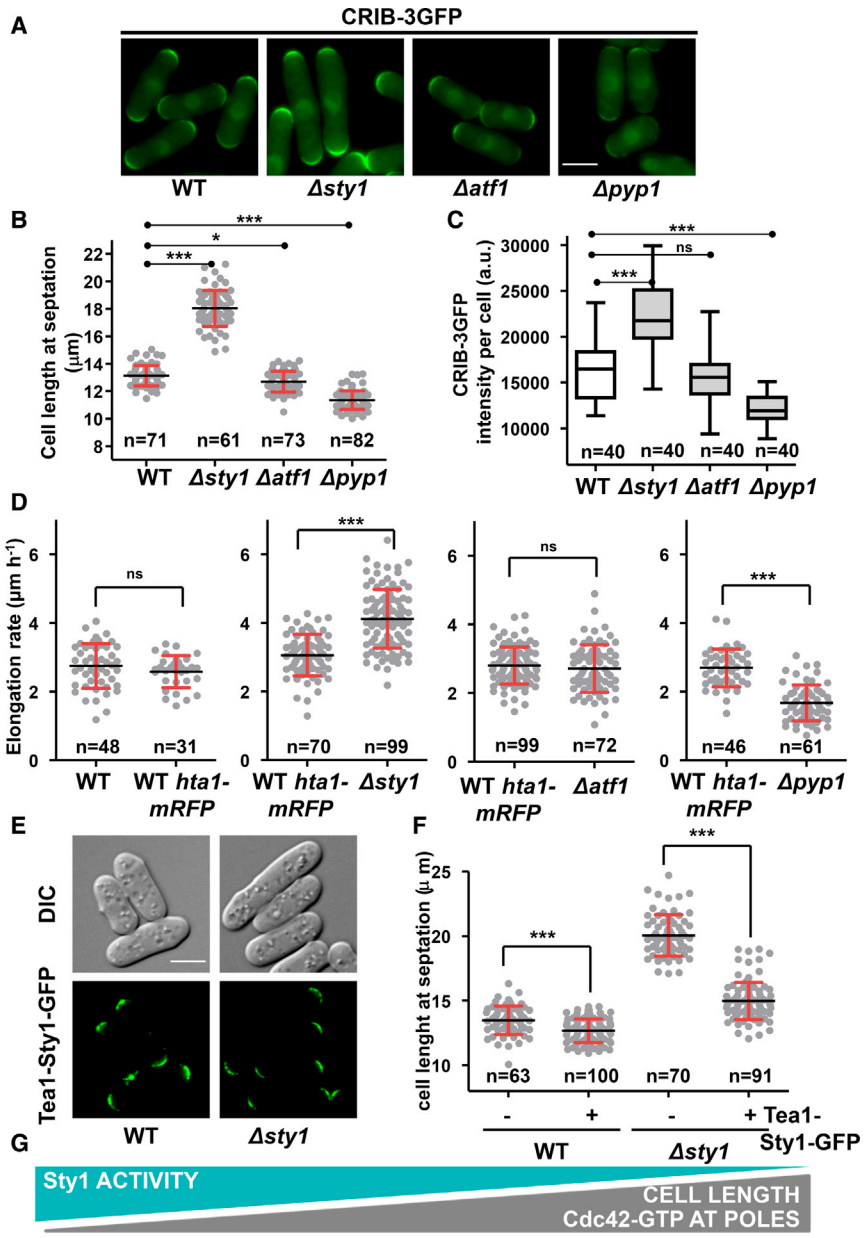

Figure 4. Cell length and Cdc42 activation at the poles are inversely correlated with Sty1 activity

(A) CRIB levels at cell tips are inversely correlated with Sty1 activation. Images of from logarithmic YE cultures of PPG65.60 (WT), CS137 (*Δsty1*), CS133 (*Δatf1*), and CS207 (*Δpyp1*) expressing CRIB-3GFP.

(B) Cell length at septation of logarithmic YE cultures of strains as in (A). Mean, SD, and number of cells analyzed (n) are indicated. Statistical significance was assessed by ANOVA test followed by Bonferroni post hoc analysis (*p < 0.05; ***p < 0.001).

(C) Quantification of CRIB intensity at cell tips of the strains shown in (A). Whiskers indicating minimum to maximum are shown, horizontal line represents mean, and n indicates the number of cells analyzed. Statistical significance was calculated as in (B) (ns, not significant).

(D) Cdc42 activity is directly related to the growth rate. Cell growth rates of MM cultures of wild-type (WT), JA1329 (wild-type cells expressing Hta1-mRFP), AV18 (*Δsty1*), MS98 (*Δatf1*), and EP48 (*Δpyp1*) were quantitated. Graphs show values distribution as in (B); statistical significance was determined using unpaired t test (***p < 0.001; *n.s.* not significant).

(E) Tea1-Sty1-GFP delivers Sty1 to cell tips. Images from MM cultures of CS309 (wild-type cells expressing the Tea1-Sty1-GFP under the *nmt81* integrative promoter) and CS310 (*Δsty1* cells expressing the same construct) are shown.

(F) Trapping Sty1 to cell tips is sufficient to restore wild-type cell size. Cell length distribution at septation of strains as in (E) was measured and is represented as in (B). Statistical significance to wild-type strain was assessed as in (B) (***p < 0.001).

(G) Schematic representation indicating the inverse proportionality between Sty1 activity and cell length and Cdc42-GTP activation at cell poles.

Scale bar, 5 μm. See also Figure S4.

Inhibition of GEF activity mediates the stress-dependent effect on growth polarity

We next tested whether inactivation or delocalization of the two *S. pombe* GEFs, Gef1 or Scd1, could mediate the Sty1-dependent inhibition of Cdc42-GTP. Cells lacking Scd1 are rounded due to its essential role in establishing sites of polarity and display weak patches of active Cdc42 (Figure S6A). In an attempt to recover cell polarity of *Δscd1* cells through the artificial tethering of either Gef1 or Scd1 to cell tips, we expressed in this background chimeras of Gef1 or Scd1 fused to Tea1. As shown in Figure 6A, both GEF-based fusion proteins, Tea1-Scd1-GFP and Tea-Gef1-GFP, when expressed in cells lacking Scd1, are localized to cell tips and able to promote the accumulation of CRIB-mCherry at the growing poles. They partially suppress the rounded phenotype of strain *Δscd1* both in length (Figure 6B) and in width (Figure S6B). With this constitutively tethered GEF-based chimeras in cells

(Figures S5C and S5D). The growth poles of double *Δrga3 Δrga6* mutant cells retain higher Cdc42 activity than single *Δrga3* cells and did not show lateral patches after H_2O_2 imposition (Figures 5E and 5F). We conclude that cells lacking the Cdc42 GAPs Rga3 and Rga6 do not display two important hallmarks linked to stress-dependent cell polarity inhibition: dispersal of CRIB-3GFP from poles and appearance of Cdc42-GTP lateral patches. Unlike cells lacking Sty1, cell growth is still inhibited by stress in *Δrga3 Δrga6* cells (Figure 5G), and the main GEF Scd1 is still dispersed from the tips upon stress in cells lacking Rga3 (Figure S5E); all of this suggests that other components of the polarity module may be also targets of the active kinase.

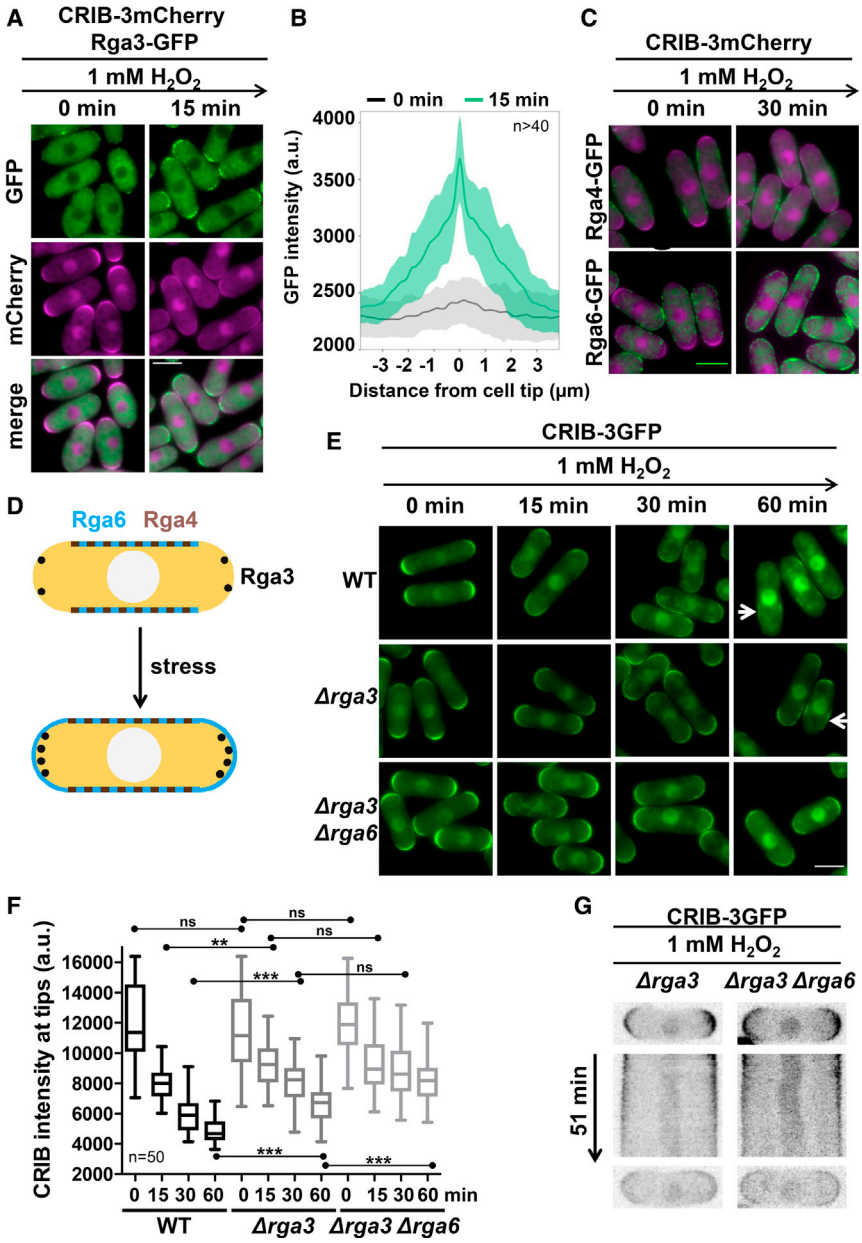

Figure 5. Cells lacking the Cdc42 GAPs Rga3 and Rga6 are insensitive to stress-dependent cell polarity inhibition

(A) Rga3 is enriched at cell poles after stress imposition. Images from logarithmic MM cultures of CS391 (expressing CRIB-3mCherry and a GFP-tagged version of Rga3 from its own locus), treated or not with 1 mM H_2O_2.

(B) Quantification of Rga3-GFP intensity along the cell tips of cells as in (A). Shaded areas represent SD, and n indicates the number of tips analyzed.

(C) Rga6 spreads to cell tips after stress imposition. Images with merged staining of GTP-bound Cdc42 (in magenta) and GFP-tagged versions of Rga4 or Rga6 (in green). YE cultures of CS361 (expressing CRIB-3mCherry and Rga4-GFP) and CS362 (expressing CRIB-3mCherry and Rga6-GFP) were treated or not with 1 mM H_2O_2.

(D) Schematic representation of GAPs cellular distribution before and after H_2O_2 imposition. See text for details.

(E) CRIB dispersal after stress imposition is blocked in cells lacking Rga3 and Rga6. Images of GTP-bound Cdc42 from YE cultures of PPG65.60, CS244, and CS315 (expressing CRIB-3GFP in wild-type, *Δrga3*, and *Δrga3 Δrga6* backgrounds, respectively) treated or not with 1 mM H_2O_2. White arrows point to lateral patches.

(F) Quantification of CRIB-3GFP intensity at cell tips of strains as in (E). Whiskers represent minimum to maximum values, horizontal lines indicate the mean, and n indicates the number of tips analyzed for each condition. Statistical analysis was performed as in Figure 4B (ns, not significant; $^{**}p < 0.01$; $^{***}p < 0.001$).

(G) Cells lacking Rga3 and Rga6 do not elongate after stress imposition. Kymographs showing CRIB-3GFP cells from time-lapse experiments as in (E).

Scale bar, 5 µm. See also Figure S5.

lacking Scd1, we tested the effect of stress on polarized growth. Probably due to the different conformation of the large chimeras, the fluorescence levels of Tea1-Scd1-GFP and Tea1-Gef1-GFP are different, but both proteins are retained at cell poles after stress imposition, as expected (Figures 6C and 6D), and the same occurs with Tea1-GFP (Figures S7A and S7B). H_2O_2 causes dispersal of active Cdc42 from the cell tips to lateral patches in *Δscd1* cells expressing Tea1-Scd1-GFP (Figures 6C and 6E), indicating that tethering Scd1 at cell poles does not prevent the inhibition of Cdc42 activity upon stress (see Figure 2A). In contrast, *Δscd1* cells expressing Tea1-Gef1-GFP are blind to stress imposition; CRIB-mCherry remains at cell tips, and lateral patches are not formed (Figures 6C and 6E). Importantly, inversion of the fluorescent tags (Tea1-Gef1-mCherry and CRIB-3GFP) in *Δscd1* cells (Figures S6C and S7C) or in a *Δgef1* background (Figure S6D) also yields stress-insensitive strains. This experiment suggests that removal of Gef1 from cell tips could be one of the molecular events leading to the stress-dependent Cdc42 inactivation in wild-type cells. In concordance, cells lacking Gef1 suffer faster stress-dependent inhibition of active Cdc42 at the poles than wild-type cells (compare 15 min after H_2O_2 imposition in both strain backgrounds in Figure 2C), and exit of Gef1-3YPF from cells tips upon stress depends on Sty1 (Figure S7D), suggesting a possible participation of this GEF in the inactivation of Cdc42 at cell tips.

Rga3, Rga6, and Gef1 are direct targets of the MAP kinase Sty1

To identify direct molecular targets of Sty1 in the polarity module, we developed an *in vitro* phosphorylation assay with

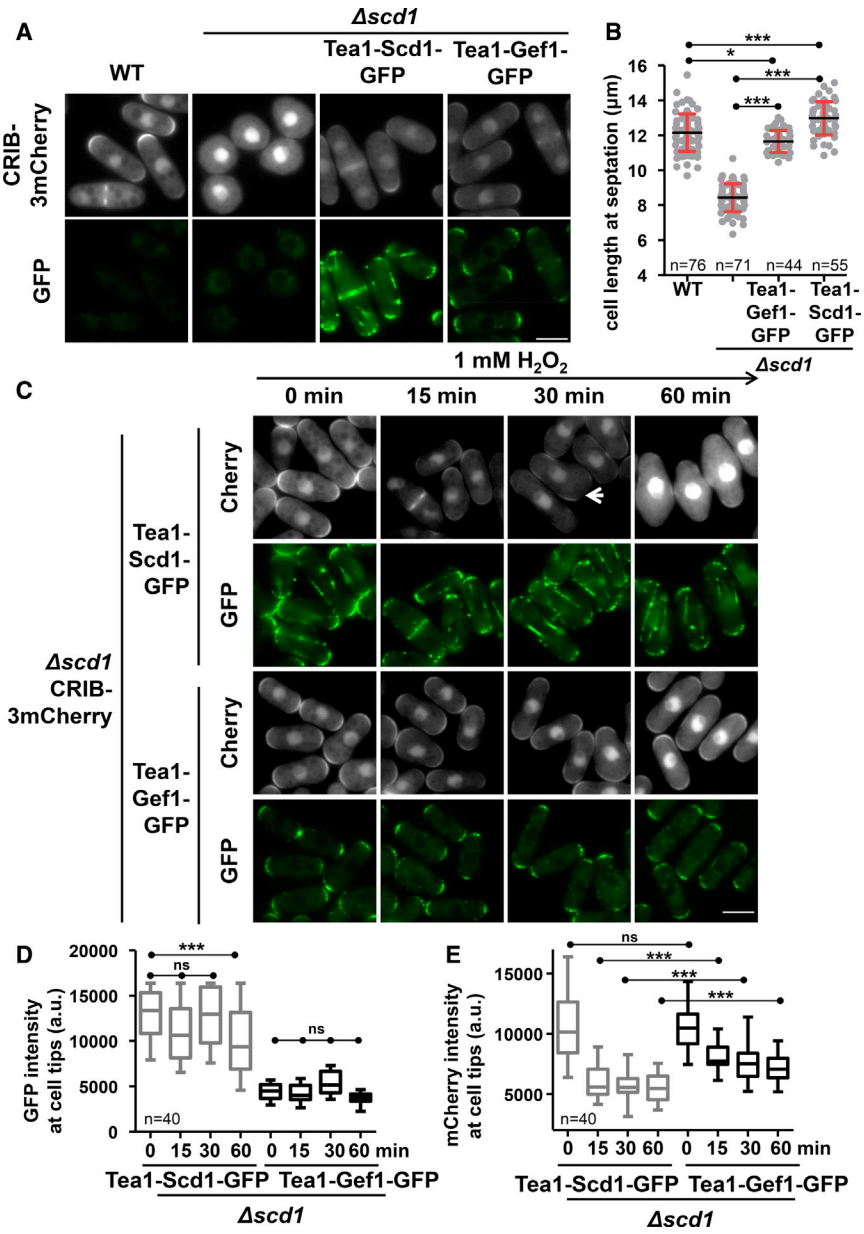

Figure 6. Trapping Gef1 to cell tips creates stress-blinded poles

(A) Trapping GEFs to cell tips restores cell morphology and GTP-Cdc42 levels in *Δscd1* cells. Images of CRIB and GFP from MM cultures of CS357, CS359 (wild-type and *Δscd1* strains, respectively, expressing CRIB-3mCherry), CS365, and CS360 (*Δscd1* strains expressing CRIB-3mCherry with Tea1-Scd1-GFP or Tea1-Gef1-GFP fusion proteins, respectively).

(B) Cell-length distribution at septation of strains as in (A). Mean, SD, and number of cells analyzed (n) are indicated. Statistical differences were calculated as in Figure 4B (*$p < 0.05$; ***$p < 0.001$).

(C) Trapping Gef1 to cell tips, but not Scd1, retains GTP-Cdc42 at tips after stress imposition. Images of CRIB and GFP from MM cultures of CS365 and CS360 treated with 1 mM H_2O_2.

(D) The Tea1-GEF-GFP fusion protein is anchored at cell tips after stress imposition. Quantification of GFP intensity at cell tips of strains as in (C), represented as in Figure 5F. Statistical analysis was performed as in Figure 4B (ns, not significant; ***$p < 0.001$).

(E) Quantification of CRIB-3mCherry intensity at cell tips of strains as in (C), represented as in (D). Scale bar, 5 μm. See also Figures S6 and S7.

recombinant proteins. We purified several recombinant chimeras fused to glutathione S-transferase (GST) in *Escherichia coli*, including the MAP kinase Sty1, a kinase-dead version Sty1.K49R (carrying a mutation in the ATP binding site), and the upstream constitutively activated version of the MAP kinase Wis1.DD (Shiozaki et al., 1998). We used as a control for the kinase reaction a bona fide substrate of Sty1, the transcription factor Atf1 (Wilkinson et al., 1996), that presents 11 MAP kinase sites (Lawrence et al., 2007). Since the GST-fused full-length Atf1 is degraded during protein purification (Figure S8A), we tested in parallel a truncated version carrying eight of the MAP kinase sites (Atf1$^{71–291}$ in Figure S8A). We also tested as substrates full-length Atf1 carrying mutations at the MAP kinase sites (10M and 10D in Figure S8A). In the kinase reaction, we first activated Sty1 with Wis1.DD in the presence of cold ATP to then add the purified substrates, Atf1 and derivatives, and γ-^{32}P-ATP. As shown in Figures 7A and S8A, when Atf1 was incubated with pre-activated Sty1, but not with the kinase-dead Sty1.K49R, the transcription factor was unambiguously phosphorylated by Sty1. Full-length or truncated Atf1 are both phosphorylated to similar extents, while the 10M and 10D mutants are barely phosphorylated in our assay at nonspecific sites, as previously reported *in vivo* (Salat-Canela et al., 2017; Sánchez-Mir et al., 2020). Recombinant GST-GFP was used as a negative substrate control (Figure S8A).

We then purified several recombinant proteins of the polarity module, including the GAPs and GEFs of Cdc42 fused to GST. The schemes of the proteins tested are shown in Figures S8B and S9C. Purified GST-tagged Rga3$^{1–447}$, containing 17 out of 20 putative MAP kinase sites (Figure S8B), and full-length Rga6 were first tested for their phosphorylation by wild-type GST-Sty1 or its catalytically dead version GST-Sty1.K49R. As shown in Figure 7B, GST-tagged Rga3$^{1–447}$, and, to a lesser extent, Rga6, are phosphorylated by wild-type GST-Sty1, but not by GST-Sty1.K49R. Based on the genetic evidences and the *in vitro* results shown above, we propose that Rga3 is a direct target of Sty1 and that its phosphorylation promotes its activation to initiate Cdc42 dispersion from the cell tips upon stress imposition.

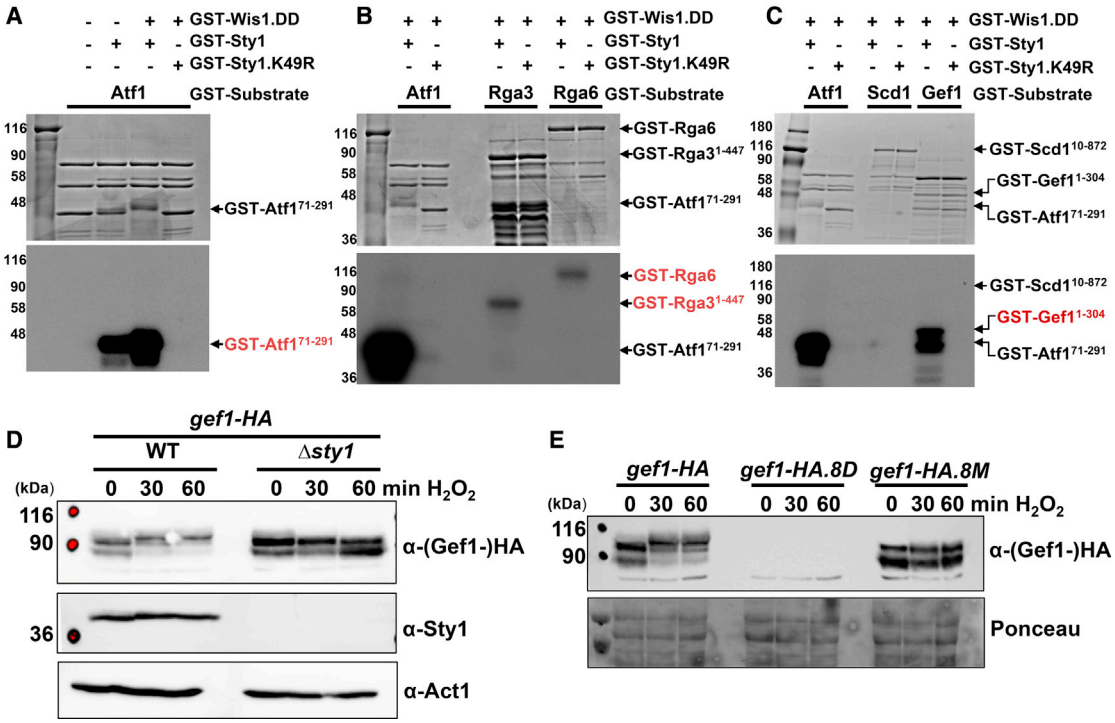

Figure 7. Rga3, Rga6, and Gef1 are phosphorylated by Sty1

(A) Sty1 activity *in vitro* is enhanced by the presence of the constitutive active MAP kinase kinase Wis1.DD. Recombinant GST-tagged Atf1$^{71–291}$ was incubated with γ-^{32}P-ATP and GST-Sty1 or GST-Sty1.K49R in the presence or absence of GST-Wis1.DD. Coomassie blue staining (top) and autoradiogram (bottom) are shown, with molecular weight markers (in kDa).

(B) Rga3 and Rga6 are substrates of Sty1 *in vitro*. GST-purified Rga3$^{1–447}$ and the full-length version of Rga6 were tested as substrates of Sty1, as in (A). Atf1$^{71–291}$ was used as a positive control.

(C) Gef1 is a substrate of Sty1 *in vitro*. GST-purified Scd1$^{10–872}$ and Gef1$^{1–304}$ were tested as substrates of Sty1, as in (A). Atf1$^{71–291}$ was used as a positive control.

(D) Gef1 is phosphorylated *in vivo* by Sty1 kinase. Trichloroacetic acid (TCA) extracts from YE cultures of CS384 and MC200 (Gef1-HA from its own locus in a wild-type or *Δsty1* background, respectively) treated with 1 mM H_2O_2 were resolved by western blotting using monoclonal antibody (anti-HA) or polyclonal antibody (anti-Sty1). Actin (α-act1) was used as a loading control.

(E) Analysis of Gef1 phosphorylation in extracts from cells expressing Gef1-HA (CS384), Gef1.8D-HA (CS384.8D), or Gef1.8M (CS384.8M). TCA extracts were processed as in (D). Ponceau staining is shown as a loading control.

See also Figures S8 and S9.

We also tested two domains of the GEFs Scd1 and Gef1 and showed that GST-Gef1$^{1–304}$, containing seven out of eight S/TP sites, is heavily phosphorylated by activated Sty1 *in vitro*, to a similar extent to the control substrate Atf1 (Figure 7C). We then tested *in vivo* Sty1-dependent Gef1 phosphorylation upon stress. Cells expressing Gef1-hemagglutinin (HA) from its own promoter were treated with H_2O_2, and extracts were tested by western blot. As shown in Figure 7D, a slower migrating band corresponding to phosphorylated Gef1-HA is evident in extracts of cells subjected to oxidative stress, which does not appear in extracts from cells lacking Sty1. We generated the hypophosphorylated and phosphomimetic versions of Gef1 by substituting the S/TP sites to non-phosphorylatable or acidic amino acids, respectively, and expressed them as GST fusions in bacteria and from their own promoter in *S. pombe.* Recombinant GST-Gef1.7M is not phosphorylated *in vitro* (Figure S9A). As shown in Figure 7E, the hypophosphorylated Gef1-HA.8M protein expressed in *S. pombe* is not phosphorylated upon stress, while the phosphomimic Gef1-HA.8D mutant is not detected. Likely this protein is very unstable; the *gef1-HA.8D* mRNA expression levels are not impaired (Figure S9B), while Gef1-HA.8D protein is undetectable in extracts.

In summary, our data demonstrate that Rga3 and Gef1 are direct targets of Sty1 *in vivo*, and we propose that their Sty1-mediated phosphorylation participates in the transient inhibition of cell growth and polarity upon stress.

DISCUSSION

Adaptation to stress includes multiple cellular responses, most of them transcriptional or resulting in cell-cycle inhibition. Signaling cascades often mediate a variety of effects through modification of diverse downstream effectors, such as transcription factors or cell-cycle regulators. Here, we describe the effect of the MAP kinase Sty1 on cell polarity. By directly regulating factors of the polarity module at the cell tips, the H_2O_2-activated kinase alters the equilibrium between GAPs and GEFs and transiently inactivates Cdc42, the driving force of the polarity module, until growth conditions are favorable again. When stress is applied, three related phenomena are observed: active

Cdc42-GTP is dispersed from cell tips, lateral patches of Cdc42-GTP are formed, and cellular growth rates are fully inhibited.

Lateral patches after Cdc42-GTP dispersal from cell tips are observed in a variety of Sty1-activating conditions, including LatA treatment (Bendezú and Martin, 2011; Hercyk et al., 2019; Mutavchiev et al., 2016), nutrient depletion (Chen et al., 2019), heat shock (Vjestica et al., 2013), osmotic stress (Haupt et al., 2018), and oxidative stress, as reported here. We show that the quaternary complex Cdc42-Pak1-Scd2-Scd1 (Lamas et al., 2020) is broken at cell tips upon stress and the scaffold protein Scd2, the downstream effector Pak1, and Gef1 are present in Cdc42-GTP lateral patches. The activation of Cdc42 at these sites uniquely relies on Gef1, as also reported in response to LatA (Hercyk et al., 2019). Scd2 is dispensable for Gef1-dependent Cdc42 activation at these lateral sites (Figure S2A). Even though Cdc42 effector proteins, including the formin For3 and components of the exocyst, are located at the lateral patches (Bendezú and Martin, 2011), Cdc42 activation at these sites does not lead to any observable morphological changes. Probably, co-localization with GAPs or the presence of downstream inhibitors or both limit further downstream activation of the Cdc42 cascade.

Upon stress imposition, a rising of the GTPase activity at cell tips could unbalance the GTP/GDP equilibrium of Cdc42 toward the inactive state. Stress-activated Sty1 limits the amount of active Cdc42 at cell tips by activating Rga3 and inhibiting Gef1, promoting cell growth arrest, and linking the activity of the module with environmental signals.

Cells lacking Rga3 display a slower Cdc42 depolarization from cell tips after H_2O_2 treatment. Basal Cdc42-GTP concentration at poles is not affected in *Δrga3* cells, indicating that a slower depolarization is not due to a higher initial concentration of Cdc42-GTP. Rga3 co-localizes with active Cdc42 at cell tips in the absence of stress (Gallo Castro and Martin, 2018), and it is further enriched at poles upon stress and inversely correlates with active Cdc42 (Figure 5A). Interestingly, budding yeast Cdc42 GAPs are also post-translationally regulated, including phosphorylation by cyclin-dependent kinases that inhibits GAP activity (Knaus et al., 2007; Sopko et al., 2007). Our experiments suggest that Rga3 functions as a "stress" GAP. Upon phosphorylation by Sty1, Rga3 rapidly promotes Cdc42-GTP hydrolysis; phosphorylation by the MAP kinase probably induces the catalytic activity of the GAP, since its recruitment to the cell tips is not abolished in cells lacking Sty1 (data not shown). Full inactivation of Cdc42 by Rga3 requires the synergistic participation of Rga6, and *Δrga3 Δrga6* cells lack the two hallmarks of Cdc42 depolarization (decrease of active Cdc42 at tips and formation of lateral patches). We propose that Rga6 collaborates with Rga3 in the Cdc42 switch-off at later stages of the stress response.

The presence and role of the two GEFs, Scd1 and Gef1, at cell poles are a matter of debate. There is no controversy regarding the prevalent function of Scd1 in polarized growth; while cells lacking Gef1 maintain the elongated phenotype of the wild-type background, *Δscd1* cells display rounded morphology (Coll et al., 2003; Chang et al., 1994). Regarding localization, while the Sawin group proposed that Gef1 is not actively enriched at membranes but is rather ubiquitously present in the cytoplasm (Tay et al., 2018), fluorescently tagged Gef1 has been reported at cell tips by several groups, including ours (Das et al., 2009, 2015; Kokkoris et al., 2014; Rincon et al., 2007; Vjestica et al., 2013). In fact, this weak but reproducible localization at the tip membrane is challenged in cells lacking Mas5 (Vjestica et al., 2013), which display higher levels of active Sty1 (Boronat et al., 2020). Despite the lack of severe morphological defects in *Δgef1* cells, a qualitative participation of this GEF in the oscillatory behavior of active Cdc42 at poles (Das et al., 2012) and in the establishment of new growth zones (Kokkoris et al., 2014) has been proposed, with Gef1 initiating Cdc42 activation at these new sites (Hercyk et al., 2019). Thus, Gef1 would have a "priming" role in the generation of the starting Cdc42-GTP molecules at a new site. Later on, Scd1, in complex with Scd2 and Pak1, would be recruited to the new site through the recognition of preexisting Cdc42-GTP as a positive feedback loop (Lamas et al., 2020). Thus, the seeding by Gef1 of new sites of polarity supports the need to switch it off when preexisting growth poles are inhibited upon stress, explaining our findings about Gef1 phosphorylation/inhibition by Sty1. Furthermore, the downregulation of Gef1 activity through phosphorylation by the kinase Orb6 and its activation by the phosphatase PP1 have already been described (Das et al., 2015; Kokkoris et al., 2014). Other Scd1-containing complex components may also be direct targets of stress. We have not been able to detect any Sty1-dependent phosphorylation of Ras1, Scd1, or Pak1 in our *in vitro* assays, but we observed a weak and reproducible phosphorylation on Scd2 (Figure S9C and S9D). Furthermore, we have recently determined that Scd1-GFP depolarizes from cell tips in a Sty1-independent manner, which opens the door to a stress-dependent Sty1-independent control of polarized growth (data not shown). Other downstream effectors of the polarity module could also be directly targeted by Sty1 to block vesicle-mediated trafficking of module components, and this is under investigation.

We have shown here that the elongated phenotype of cells lacking Sty1 is at least partly due to a hyper-activation of the Cdc42 polarity module. We envision the idea that both the stress-dependent and the basal cell size regulation of Cdc42 by Sty1 occur through the same target protein(s) and that Cdc42 activity may be controlled by Sty1-mediated regulatory mechanisms during unperturbed mitotic growth: to initiate growth at the new pole, to proceed with cytokinesis or for mating during sexual reproduction. Indeed, cells lacking Sty1 have severe defects associated with those processes, which could be connected to Cdc42 activity. Further work will be required to fully understand the relationship between Sty1 and unperturbed cell-cycle events and extrapolate our main finding, the connection of the stress-dependent pathway with cell growth and polarity, to other eukaryotic model systems.

Limitations of the study

We have used genetic and biochemical approaches to study the inhibition of the Cdc42 polarity module by Sty1. The activity of this kinase inversely correlates with active Cdc42 at tips and with cell length, and we propose that this explains the elongated morphology of *Δsty1* cells, without ruling out a direct role of the kinase on cell-cycle regulation. We have created stress-blinded cells by eliminating two Cdc42 GAPs or through the constitutive tethering of Gef1 to cell tips, and *in vitro* phosphorylation assays

support the notion that the GAPs Rga3/6 and the GEF Gef1 are direct substrates of Sty1. However, we suspect that H_2O_2 causes a combination of events, with other targets still to be discovered, to fully inhibit polarized growth, and our genetic analyses suggest that synergy between them occurs. Those events probably cross-talk, and eliminating one of them may be minimized by compensatory effects on the others, anticipating a difficult interpretation of genetic data.

STAR★METHODS

Detailed methods are provided in the online version of this paper and include the following:

- KEY RESOURCES TABLE
- RESOURCE AVAILABILITY
  - Lead contact
  - Materials availability
  - Data and code availability
- EXPERIMENTAL MODEL AND SUBJECT DETAILS
- METHOD DETAILS
  - Yeast strains, plasmids and molecular biology
  - Drug treatments
  - Microscopy techniques and image processing
  - Elongation rates assay using FITC
  - H_2O_2 sensitivity assay
  - TCA extracts and immuno blot analysis
  - Protein production in *E. coli*
  - *In vitro* kinase assay
  - Protein sequence analysis
- QUANTIFICATION AND STATISTICAL ANALYSIS

SUPPLEMENTAL INFORMATION

Supplemental information can be found online at https://doi.org/10.1016/j.celrep.2021.109951.

ACKNOWLEDGMENTS

We thank Paul Nurse, James Moseley, Mohan Balasubramanian, and Fulvia Verde for sharing strains and plasmids. We also thank Danny Lew and Rong Li for kindly sharing plasmids to express CDC24 in *S. pombe*. We are especially thankful to Aleksandar Vjestica and Sophie Martin for helpful discussions and the generation and generous sharing of several fission yeast genetic tools, as well as NBRP (YGRC; Japan) for their distribution. We thank Margarita Cabrera, Javier Encinar del Dedo, and the UPF-CRG Microscopy facility for technical support with image acquisition and analysis. This work is supported by the Ministerio de Ciencia, Innovación y Universidades (Spain), PLAN E, and FEDER (grant PGC2018-093920-B-I00 to E.H., PGC2018-097248-B-I00 to J.A., and PGC2018-098924-B-100 to P.P.). The Oxidative Stress and Cell Cycle group is also supported by Generalitat de Catalunya (Spain) (2017-SGR-539) and Unidad de Excelencia María de Maeztu, funded by the AEI (Spain) (grant CEX2018-000792-M). P.P. is also supported by Junta de Castilla y León (Escalera de la Excelencia) (grant CLU-2017-03). C.S.-C. was recipient of a María de Maeztu predoctoral fellowship from the Ministerio de Economía y Competitividad (Spain).

AUTHOR CONTRIBUTIONS

C.S.-C., M.C., and R.M.-G. performed the experiments. C.S.-C., J.A., P.P., and E.H. analyzed the data. E.H. and C.S.-C. wrote the manuscript.

DECLARATION OF INTERESTS

The authors declare no competing interests.

Received: February 4, 2021
Revised: July 20, 2021
Accepted: October 14, 2021
Published: November 2, 2021

SUPPORTING CITATIONS

The following reference appears in the supplemental information: Fernández-Vázquez et al. (2013), Leupold (1970), and Zuin et al. (2005).

REFERENCES

Alfa, C., Fantes, P., Hyams, J., McLeod, M., and Warbrick, E. (1993). Experiments with Fission Yeast: A Laboratory Course Manual (New York: Cold Spring Harbor).

Bendezú, F.O., and Martin, S.G. (2011). Actin cables and the exocyst form two independent morphogenesis pathways in the fission yeast. Mol. Biol. Cell *22*, 44–53.

Bendezú, F.O., Vincenzetti, V., Vavylonis, D., Wyss, R., Vogel, H., and Martin, S.G. (2015). Spontaneous Cdc42 polarization independent of GDI-mediated extraction and actin-based trafficking. PLoS Biol. *13*, e1002097.

Bohnert, K.A., Rossi, A.M., Jin, Q.W., Chen, J.S., and Gould, K.L. (2020). Phosphoregulation of the cytokinetic protein Fic1 contributes to fission yeast growth polarity establishment. J. Cell Sci. *133*, jcs244392.

Boronat, S., Marte, L., Vega, M., García-Santamarina, S., Cabrera, M., Ayté, J., and Hidalgo, E. (2020). The Hsp40 Mas5 connects protein quality control and the general stress reesponse through the thermo-sensitive Pyp1. iScience *23*, 101725.

Calvo, I.A., Gabrielli, N., Iglesias-Baena, I., García-Santamarina, S., Hoe, K.L., Kim, D.U., Sansó, M., Zuin, A., Pérez, P., Ayté, J., and Hidalgo, E. (2009). Genome-wide screen of genes required for caffeine tolerance in fission yeast. PLoS ONE *4*, e6619.

Chang, E.C., Barr, M., Wang, Y., Jung, V., Xu, H.P., and Wigler, M.H. (1994). Cooperative interaction of S. pombe proteins required for mating and morphogenesis. Cell *79*, 131–141.

Chen, D., Toone, W.M., Mata, J., Lyne, R., Burns, G., Kivinen, K., Brazma, A., Jones, N., and Bähler, J. (2003). Global transcriptional responses of fission yeast to environmental stress. Mol. Biol. Cell *14*, 214–229.

Chen, D., Wilkinson, C.R., Watt, S., Penkett, C.J., Toone, W.M., Jones, N., and Bähler, J. (2008). Multiple pathways differentially regulate global oxidative stress responses in fission yeast. Mol. Biol. Cell *19*, 308–317.

Chen, C., Rodriguez Pino, M., Haller, P.R., and Verde, F. (2019). Conserved NDR/LATS kinase controls RAS GTPase activity to regulate cell growth and chronological lifespan. Mol. Biol. Cell *30*, 2598–2616.

Chiou, J.G., Balasubramanian, M.K., and Lew, D.J. (2017). Cell Polarity in Yeast. Annu. Rev. Cell Dev. Biol. *33*, 77–101.

Coll, P.M., Trillo, Y., Ametzazurra, A., and Perez, P. (2003). Gef1p, a new guanine nucleotide exchange factor for Cdc42p, regulates polarity in Schizosaccharomyces pombe. Mol. Biol. Cell *14*, 313–323.

Das, M., Wiley, D.J., Medina, S., Vincent, H.A., Larrea, M., Oriolo, A., and Verde, F. (2007). Regulation of cell diameter, For3p localization, and cell symmetry by fission yeast Rho-GAP Rga4p. Mol. Biol. Cell *18*, 2090–2101.

Das, M., Wiley, D.J., Chen, X., Shah, K., and Verde, F. (2009). The conserved NDR kinase Orb6 controls polarized cell growth by spatial regulation of the small GTPase Cdc42. Curr. Biol. *19*, 1314–1319.

Das, M., Drake, T., Wiley, D.J., Buchwald, P., Vavylonis, D., and Verde, F. (2012). Oscillatory dynamics of Cdc42 GTPase in the control of polarized growth. Science *337*, 239–243.

Das, M., Nuñez, I., Rodriguez, M., Wiley, D.J., Rodriguez, J., Sarkeshik, A., Yates, J.R., 3rd, Buchwald, P., and Verde, F. (2015). Phosphorylation-

dependent inhibition of Cdc42 GEF Gef1 by 14-3-3 protein Rad24 spatially regulates Cdc42 GTPase activity and oscillatory dynamics during cell morphogenesis. Mol. Biol. Cell *26*, 3520–3534.

Estravís, M., Rincón, S.A., Portales, E., Pérez, P., and Santos, B. (2017). Cdc42 activation state affects its localization and protein levels in fission yeast. Microbiology (Reading) *163*, 1156–1166.

Fernández-Vázquez, J., Vargas-Pérez, I., Sansó, M., Buhne, K., Carmona, M., Paulo, E., Hermand, D., Rodríguez-Gabriel, M., Ayté, J., Leidel, S., and Hidalgo, E. (2013). Modification of tRNA(Lys) UUU by elongator is essential for efficient translation of stress mRNAs. PLoS Genet. *9*, e1003647.

Gallo Castro, D., and Martin, S.G. (2018). Differential GAP requirement for Cdc42-GTP polarization during proliferation and sexual reproduction. J. Cell Biol. *217*, 4215–4229.

Gregan, J., Zhang, C., Rumpf, C., Cipak, L., Li, Z., Uluocak, P., Nasmyth, K., and Shokat, K.M. (2007). Construction of conditional analog-sensitive kinase alleles in the fission yeast Schizosaccharomyces pombe. Nat. Protoc. *2*, 2996–3000.

Gulli, M.P., Jaquenoud, M., Shimada, Y., Niederhäuser, G., Wiget, P., and Peter, M. (2000). Phosphorylation of the Cdc42 exchange factor Cdc24 by the PAK-like kinase Cla4 may regulate polarized growth in yeast. Mol. Cell *6*, 1155–1167.

Haupt, A., Ershov, D., and Minc, N. (2018). A Positive Feedback between Growth and Polarity Provides Directional Persistency and Flexibility to the Process of Tip Growth. Curr. Biol. *28*, 3342–3351.e3.

Hercyk, B.S., Rich-Robinson, J., Mitoubsi, A.S., Harrell, M.A., and Das, M.E. (2019). A novel interplay between GEFs orchestrates Cdc42 activity during cell polarity and cytokinesis in fission yeast. J. Cell Sci. *132*, jcs236018.

Hirota, K., Tanaka, K., Ohta, K., and Yamamoto, M. (2003). Gef1p and Scd1p, the Two GDP-GTP exchange factors for Cdc42p, form a ring structure that shrinks during cytokinesis in Schizosaccharomyces pombe. Mol. Biol. Cell *14*, 3617–3627.

Huang, J., Huang, Y., Yu, H., Subramanian, D., Padmanabhan, A., Thadani, R., Tao, Y., Tang, X., Wedlich-Soldner, R., and Balasubramanian, M.K. (2012). Nonmedially assembled F-actin cables incorporate into the actomyosin ring in fission yeast. J. Cell Biol. *199*, 831–847.

Jara, M., Vivancos, A.P., Calvo, I.A., Moldón, A., Sansó, M., and Hidalgo, E. (2007). The peroxiredoxin Tpx1 is essential as a H2O2 scavenger during aerobic growth in fission yeast. Mol. Biol. Cell *18*, 2288–2295.

Kelly, F.D., and Nurse, P. (2011). Spatial control of Cdc42 activation determines cell width in fission yeast. Mol. Biol. Cell *22*, 3801–3811.

Knaus, M., Pelli-Gulli, M.P., van Drogen, F., Springer, S., Jaquenoud, M., and Peter, M. (2007). Phosphorylation of Bem2p and Bem3p may contribute to local activation of Cdc42p at bud emergence. EMBO J. *26*, 4501–4513.

Kokkoris, K., Gallo Castro, D., and Martin, S.G. (2014). The Tea4-PP1 landmark promotes local growth by dual Cdc42 GEF recruitment and GAP exclusion. J. Cell Sci. *127*, 2005–2016.

Kuo, C.C., Savage, N.S., Chen, H., Wu, C.F., Zyla, T.R., and Lew, D.J. (2014). Inhibitory GEF phosphorylation provides negative feedback in the yeast polarity circuit. Curr. Biol. *24*, 753–759.

Lamas, I., Merlini, L., Vještica, A., Vincenzetti, V., and Martin, S.G. (2020). Optogenetics reveals Cdc42 local activation by scaffold-mediated positive feedback and Ras GTPase. PLoS Biol. *18*, e3000600.

Lawrence, C.L., Maekawa, H., Worthington, J.L., Reiter, W., Wilkinson, C.R., and Jones, N. (2007). Regulation of Schizosaccharomyces pombe Atf1 protein levels by Sty1-mediated phosphorylation and heterodimerization with Pcr1. J. Biol. Chem. *282*, 5160–5170.

Leupold, U. (1970). Genetical methods for *Schizosaccharomyces pombe*. Methods Cell Physiol. *4*, 169–177.

Magliozzi, J.O., Sears, J., Cressey, L., Brady, M., Opalko, H.E., Kettenbach, A.N., and Moseley, J.B. (2020). Fission yeast Pak1 phosphorylates anillin-like Mid1 for spatial control of cytokinesis. J. Cell Biol. *219*, e201908017.

Martin, S.G. (2015). Spontaneous cell polarization: Feedback control of Cdc42 GTPase breaks cellular symmetry. BioEssays *37*, 1193–1201.

Mata, J., and Nurse, P. (1997). tea1 and the microtubular cytoskeleton are important for generating global spatial order within the fission yeast cell. Cell *89*, 939–949.

Millar, J.B., Buck, V., and Wilkinson, M.G. (1995). Pyp1 and Pyp2 PTPases dephosphorylate an osmosensing MAP kinase controlling cell size at division in fission yeast. Genes Dev. *9*, 2117–2130.

Miller, P.J., and Johnson, D.I. (1994). Cdc42p GTPase is involved in controlling polarized cell growth in Schizosaccharomyces pombe. Mol. Cell. Biol. *14*, 1075–1083.

Mitchison, J.M., and Nurse, P. (1985). Growth in cell length in the fission yeast Schizosaccharomyces pombe. J. Cell Sci. *75*, 357–376.

Mutavchiev, D.R., Leda, M., and Sawin, K.E. (2016). Remodeling of the Fission Yeast Cdc42 Cell-Polarity Module via the Sty1 p38 Stress-Activated Protein Kinase Pathway. Curr. Biol. *26*, 2921–2928.

Ozbudak, E.M., Becskei, A., and van Oudenaarden, A. (2005). A system of counteracting feedback loops regulates Cdc42p activity during spontaneous cell polarization. Dev. Cell *9*, 565–571.

Paulo, E., García-Santamarina, S., Calvo, I.A., Carmona, M., Boronat, S., Domènech, A., Ayté, J., and Hidalgo, E. (2014). A genetic approach to study H2O2 scavenging in fission yeast–distinct roles of peroxiredoxin and catalase. Mol. Microbiol. *92*, 246–257.

Rapali, P., Mitteau, R., Braun, C., Massoni-Laporte, A., Ünlü, C., Bataille, L., Arramon, F.S., Gygi, S.P., and McCusker, D. (2017). Scaffold-mediated gating of Cdc42 signalling flux. eLife *6*, e25257.

Revilla-Guarinos, M.T., Martin-Garcia, R., Villar-Tajadura, M.A., Estravis, M., Coll, P.M., and Perez, P. (2016). Rga6 is a Fission Yeast Rho GAP Involved in Cdc42 Regulation of Polarized Growth. Mol. Biol. Cell. *27*, 1524–1535.

Rincon, S., Coll, P.M., and Perez, P. (2007). Spatial regulation of Cdc42 during cytokinesis. Cell Cycle *6*, 1687–1691.

Salat-Canela, C., Paulo, E., Sánchez-Mir, L., Carmona, M., Ayté, J., Oliva, B., and Hidalgo, E. (2017). Deciphering the role of the signal- and Sty1 kinase-dependent phosphorylation of the stress-responsive transcription factor Atf1 on gene activation. J. Biol. Chem. *292*, 13635–13644.

Sánchez-Mir, L., Fraile, R., Ayté, J., and Hidalgo, E. (2020). Phosphorylation of the Transcription Factor Atf1 at Multiple Sites by the MAP Kinase Sty1 Controls Homologous Recombination and Transcription. J. Mol. Biol. *432*, 5430–5446.

Sansó, M., Gogol, M., Ayté, J., Seidel, C., and Hidalgo, E. (2008). Transcription factors Pcr1 and Atf1 have distinct roles in stress- and Sty1-dependent gene regulation. Eukaryot. Cell *7*, 826–835.

Schindelin, J., Arganda-Carreras, I., Frise, E., Kaynig, V., Longair, M., Pietzsch, T., Preibisch, S., Rueden, C., Saalfeld, S., Schmid, B., et al. (2012). Fiji: an open-source platform for biological-image analysis. Nat. Methods *9*, 676–682.

Shiozaki, K., and Russell, P. (1995a). Cell-cycle control linked to extracellular environment by MAP kinase pathway in fission yeast. Nature *378*, 739–743.

Shiozaki, K., and Russell, P. (1995b). Counteractive roles of protein phosphatase 2C (PP2C) and a MAP kinase kinase homolog in the osmoregulation of fission yeast. EMBO J. *14*, 492–502.

Shiozaki, K., Shiozaki, M., and Russell, P. (1998). Heat stress activates fission yeast Spc1/Styl MAPK by a MEKK-independent mechanism. Mol. Biol. Cell *9*, 1339–1349.

Sopko, R., Huang, D., Smith, J.C., Figeys, D., and Andrews, B.J. (2007). Activation of the Cdc42p GTPase by cyclin-dependent protein kinases in budding yeast. EMBO J. *26*, 4487–4500.

Tatebe, H., Nakano, K., Maximo, R., and Shiozaki, K. (2008). Pom1 DYRK regulates localization of the Rga4 GAP to ensure bipolar activation of Cdc42 in fission yeast. Curr. Biol. *18*, 322–330.

Tay, Y.D., Leda, M., Goryachev, A.B., and Sawin, K.E. (2018). Local and global Cdc42 guanine nucleotide exchange factors for fission yeast cell polarity are coordinated by microtubules and the Tea1-Tea4-Pom1 axis. J. Cell Sci. *131*, jcs216580.

Toone, W.M., Kuge, S., Samuels, M., Morgan, B.A., Toda, T., and Jones, N. (1998). Regulation of the fission yeast transcription factor Pap1 by oxidative

stress: requirement for the nuclear export factor Crm1 (Exportin) and the stress-activated MAP kinase Sty1/Spc1. Genes Dev. *12*, 1453–1463.

Vjestica, A., Zhang, D., Liu, J., and Oliferenko, S. (2013). Hsp70-Hsp40 chaperone complex functions in controlling polarized growth by repressing Hsf1-driven heat stress-associated transcription. PLoS Genet. *9*, e1003886.

Vještica, A., Marek, M., Nkosi, P.J., Merlini, L., Liu, G., Bérard, M., Billault-Chaumartin, I., and Martin, S.G. (2020). A toolbox of stable integration vectors in the fission yeast *Schizosaccharomyces pombe*. J. Cell Sci. *133*, jcs240754.

Wai, S.C., Gerber, S.A., and Li, R. (2009). Multisite phosphorylation of the guanine nucleotide exchange factor Cdc24 during yeast cell polarization. PLoS ONE *4*, e6563.

Wilkinson, M.G., Samuels, M., Takeda, T., Toone, W.M., Shieh, J.C., Toda, T., Millar, J.B., and Jones, N. (1996). The Atf1 transcription factor is a target for the Sty1 stress-activated MAP kinase pathway in fission yeast. Genes Dev. *10*, 2289–2301.

Zuin, A., Vivancos, A.P., Sansó, M., Takatsume, Y., Ayté, J., Inoue, Y., and Hidalgo, E. (2005). The glycolytic metabolite methylglyoxal activates Pap1 and Sty1 stress responses in Schizosaccharomyces pombe. J. Biol. Chem. *280*, 36708–36713.

Zuin, A., Carmona, M., Morales-Ivorra, I., Gabrielli, N., Vivancos, A.P., Ayté, J., and Hidalgo, E. (2010). Lifespan extension by calorie restriction relies on the Sty1 MAP kinase stress pathway. EMBO J. *29*, 981–991.

STAR★METHODS

KEY RESOURCES TABLE

REAGENT or RESOURCE	SOURCE	IDENTIFIER
Antibodies		
Anti-Atf1 polyclonal	Laboratory made	N/A
Anti-HA monoclonal	Laboratory made	12CA5
Anti-GFP	Takara	632381; RRID:AB_2313808
Anti-Sty1 monoclonal	Laboratory made	N/A
Anti-Tubulin	Sigma	T5168; RRID:AB_477579
Bacterial and virus strains		
E. coli DH5a	N/A	N/A
E. coli FB810	N/A	N/A
Chemicals, peptides, and recombinant proteins		
Ampicillin	Roche	10 835 269 001
ATP	Promega	E6011
Calcofluor	Sigma	F3543
FITC-lectin	Sigma	L9381
Hydrogen peroxide	Sigma	H1009
IPTG	Merck	I6758
Latrunculin A	Sigma	L5163
Lectin from *glycine max soybean*	Sigma	L1395
γ-^{32}P-ATP	PerkinElmer	BLU002Z250UC
TCA	VWR	1,00807,0250
Thiamine	Merck	T1270
1-NM-PP1	TRC	A603003
3-MB-PP1	TRC	A602960
Critical commercial assays		
Coomassie Brilliant Blue	Amresco	0472
Glutathione Sepharose beads	GE Healthcare	17-0756-01
GSH	Sigma	4251
Deposited data		
Raw data of images	This paper	Mendeley data: https://doi.org/10.17632/gb9zrjpt92.1
Experimental models: Organisms/strains		
Yeast strains	See Table S1	N/A
Recombinant DNA		
pARC2080		Kelly and Nurse, 2011
pJK148-Gef1-HA		This study
pAV0756		Vještica et al., 2020
GST-Pak1.K415R		Magliozzi et al., 2020
GST-Atf1$^{71-291}$		This study
p109	pGEX-4T-1-Sty1	This study
p109.K49R	pGEX-4T-1-Sty1.K49R	This study
p422	psty1:ctt1	Paulo et al., 2014
p696.81	pnmt81:Tea1	This study
p697.81	pnmt81:Tea1-(linker)-GFP	This study

(*Continued on next page*)

Continued

REAGENT or RESOURCE	SOURCE	IDENTIFIER
p701.81'	pnmt81':Tea1-(linker)-GFP	This study
p712.81'	pnmt81':Tea1-Sty1-(linker)-GFP	This study
p717.81'	pnmt81':Tea1-Gef1-(linker)-GFP	This study
p734.81'	pnmt81':Tea1	This study
p747.81'	pnmt81':Tea1-Scd1-(linker)-GFP	This study
p748.81'	pnmt81':Tea1-mCherry	This study
p755	pGEX-4T-1-Rga3$^{1-447}$	This study
p758	pGEX-4T-1-Scd1$^{10-872}$	This study
p761	pGEX-4T-1-Gef1$^{1-304}$	This study
p759	pGEX-4T-1-Rga6	This study
p771	pGEX-4T-1-Atf1	This study
p771.10D	pGEX-4T-1-Atf1.10D	This study
p771.10M	pGEX-4T-1-Atf1.10M	This study
p772	pGEX-4T-1-GFP	This study
p773	pGEX-4T-2-Wis1.DD	This study
p775.8D'	pgef1':gef1.8D-HA	This study
p775.8M'	pgef1':gef1.8M-HA	This study
p777	pGEX-4T-1-Ras1$^{3-217}$	This study
p780	pGEX-4T-1-Scd2$^{4-534}$	This study
Software and algorithms		
Adobe Illustrator 2021	Adobe	N/A
FiJi-ImageJ	NIH	https://imagej.net/software/fiji/
Gen5 software	Biotek	N/A
GraphPad Prism (6.0c)	GraphPad Software	https://www.graphpad.com/
Metamorph 7.8.13	Gataca Systems	N/A
R studio	N/A	https://www.rstudio.com
SMART	EMBL Heidelberg	http://SMART.embl-heidelberg.de
SoftWoRx 5.5.0	Applied Precision	N/A
Other		
8-chamber coverglass slides	Thermo Scientific	155411
35 mm Dish coverslip	MatTek	P35G-1.5-14-C
1 ml transfer pipette	FisherBrand	13469118

RESOURCE AVAILABILITY

Lead contact

Further information and requests for resources should be directed to and will be fulfilled by the Lead Contact, Elena Hidalgo (elena.hidalgo@upf.edu).

Materials availability

All unique reagents generated in this study are available from the Lead Contact without restriction.

Data and code availability

- All images included in the main and supplemental figures have been deposited at Mendeley and are publicly available as of the date of publication. The DOI is listed in the key resources table.
- This paper does not report original code.
- Any additional information required to reanalyze the data reported in this paper is available from the lead contact upon request.

EXPERIMENTAL MODEL AND SUBJECT DETAILS

Fission yeast strains were grown in rich medium (yeast extract, YE) or minimal medium (MM) at 30°C as described previously (Alfa et al., 1993). The genotypes of strains used in this study are shown in Table S1.

METHOD DETAILS

Yeast strains, plasmids and molecular biology

Yeast strains were constructed by standard genetic methods. Origins and genotypes of strains used in this study are described in Table S1.

Strains under the control of thiamine-repressible *nmt81* promoter were grown under the presence of 0.02 mg/ml thiamine until saturation. In order to induce gene expression, a small volume of this culture was diluted in MM media and cells were let to grow for 16 hours.

E. coli DH5α was used as a host for propagation and construction of the plasmids used in this study. Bacteria were grown in LB medium supplemented with 0.1 mg/ml ampicillin. Plasmid p422′ (Paulo et al., 2014), containing the *ctt1* gene under the control of the constitutive *sty1* promoter, was linearized and integrated by homologous recombination at the *leu1-32* locus of different strain backgrounds. To create Tea1 protein fusions, we PCR-amplified genomic *tea1* and cloned it into an episomal *nmt81*-driven background, yielding p696.81. Next, a PCR product containing a linker region followed by a GFP molecule was amplified from pARC2080, which was kindly provided by Paul Nurse (Kelly and Nurse, 2011) and cloned into the previous plasmid generating the episomal plasmid p697.81. The resulting *nmt81-tea1-(linker)-GFP* was cloned into an integrative background yielding plasmid p701.81'. A BamHI restriction site located in frame between *tea1* and the *(linker)-GFP* coding sequence (CDS) was used to clone PCR-amplified *sty1* CDS, yielding p712.81', and *gef1* CDS, yielding p717.81'. Since *scd1* CDS contains an internal BamHI site, compatible ends were generated by BglII digestion and cloned into BamHI -linearized p701.81, yielding the plasmid p747.81'. All these constructions were linearized and integrated by homologous recombination at the *leu1-32* locus of different strain backgrounds. Constructions were checked by sequencing. *tea1* CDS contains codon changes causing I359V and T983A mutations that were generated during PCR amplification. Tea1-mCherry constructions were created using a similar approach. *tea1* CDS was isolated from p696.81 and cloned into an integrative vector, yielding p734.81'. *mCherry* CDS was amplified by PCR and cloned into the previous plasmid using BamHI/SmaI enzymes. The resulting plasmid codes for integrative *nmt81*-driven Tea1-mCherry. As previously described, a BamHI restriction site located in frame between *tea1* and *mCherry* was used to clone *gef1* CDS, yielding p748.81', which was linearized and inserted by homologous recombination at the *leu1-32* locus. The plasmid pJK148-Gef1-HA (Coll et al., 2003) was linearized with XbaI to be inserted in the *gef1* locus. To generate the phosphomutant versions Gef1.8D (containing the substitutions of S14D, T97E, T100E, T140E, S167D, S246D, T284E and T480E) and Gef1.8M (S14A, T97I, T100I, T140I, S167A, S246A, T284I and T480I), the whole mutated ORF sequences were obtained from Integrated DNA Technologies (IDT) and cloned into pJK148-Gef1-HA using BglII and NotI, yielding p775'.8D and p775'.8M. In order to express GST-tagged proteins, full-length wild-type version of Atf1, the phosphomutants Atf1.10D and Atf1.10M or a truncated version (from amino acid 71 to 291), the CDSs were amplified by PCR and cloned into pGEX-4T-1 using BglII/SmaI, yielding p771, p771.10D, p771.10M and GST-Atf171-291. Similarly, the wild-type version of *sty1* gene and the kinetic mutant version *sty1.K49R* were PCR-amplified and cloned into pGEX-4T-1 using BamHI/EcoRI, yielding p109 and p109.K49R. The CDS coding for the constitutive active version of Wis1, Wis1.DD, was amplified by PCR and cloned into pGEX-4T-2 using XhoI, yielding p773. In order to be used as a negative control, the *GFP* coding sequence preceded by a linker region was amplified from pARC2080 and cloned into pGEX-4T-1 using BamHI/SmaI, yielding p772. The full-length ORF of *rga6* was PCR-amplified and cloned into pGEX-4T-1 using EcoRI/SmaI, yielding p759. The CDSs coding for fragments of $Rga3^{1-447}$, $Scd1^{10-872}$, $Gef1^{1-304}$ and $Gef1.7M^{1-304}$ were amplified by PCR and cloned into pGEX-4T-1 using BamHI/SmaI, yielding p755, p758 and p761, respectively. The CDSs coding for fragments $Ras1^{3-219}$ and $Scd2^{4-536}$ were amplified by PCR and cloned into pGEX-4T-1 using BamHI/SmaI, yielding p777 and p780, respectively. The plasmid coding for GST-Pak1.K415R was kindly provided by James Moseley (Magliozzi et al., 2020). pAV0756 coding for stable-integrative version of CRIB-3mCherry was obtained from the Japanese National BioResource Project (NBTP; https://yeast.nig.ac.jp/yeast) and cloned at the wild-type *his5* locus as described elsewhere (Vještica et al., 2020).

Drug treatments

Cells were incubated with H_2O_2 and LatA purchased from Sigma (H1009 and L5163, respectively) at the indicated concentrations. ATP-analogs 1-NM-PP1 and 3-MB-PP1 were obtained from Toronto Research Chemicals (A603003; A602960).

Microscopy techniques and image processing

Cells were grown to logarithmic phase in either YE or MM, as indicated in each figure legend. For time-lapse experiments, 8-chamber coverglass slides (155411, Thermo Scientific) or Petri dishes with glass bottom coverslip (MatTek, P35G-1.5-14-C) were coated with 1 mg/ml of lectin from glycine max soybean (L1395, Sigma) and left for 30 min. Excess of lectin was washed with appropriate medium and 200 μl of cell culture was added to each chamber and left to settle for 2 min. Next, the cells were washed once with appropriate media and the same volume of pre-warmed fresh media was added. The preparations were placed at the microscope chamber at

30°C, except for experiments involving pretreatment with 3MB-PP1. In that case, media containing the drug was added and the chamber was left for 60 min in a 30°C incubator. We realized that the use of other ATP analogs such as the 1NM-PP1 or 3Br-PP1 had an inhibitory effect on the wild-type version of the Sty1 kinase, and probably other kinases (data not shown), as described elsewhere (Bohnert et al., 2020). For that reason, we strongly recommend the use of 3MB-PP1 with the analog sensitive version of Sty1 kinase, Sty1.T97A. For time-lapse experiments (as in Figures 1A, 1C, 2A, 2C, 5G, and S3C) we used a spinning disk confocal microscope (Revolution XD; Andor Technology) with a Plan Apochromat 100 × , 1.45 NA objective equipped with a dual-mode electron-modifying charge-coupled device camera (iXon 897 E; Andor Technology). Seventeen z stacks along 4 μm were acquired every 3 min for CRIB-GFP cells and every 6 min for CRIB-dTomato cells. iQ Live Cell Imaging software (Andor Technology) was used for image acquisition. For the addition of either LatA or H_2O_2 during imaging, media was removed carefully using a 1 ml transfer pipette (13469118, FisherBrand) and the same amount of media containing the appropriate compound was added. This process was completed within a 3 min time interval so the acquisition timing was not disrupted. For time-lapse experiments (as shown in Figure 3F), Petri dishes were kept at 30°C using an Okolab stage top chamber on a Nikon Eclipse Ti2 microscope fused to an Andor Dragonfly spinning disk unit equipped with a 488nm laser, using a U Plan Apo 60x 1.4 oil objective and an iXON-EMCCD Du-897 camera. A 2x camera zoom was used to reach Nyquist sampling. In this case, three z stacks along 2 μm were acquired every 6 min. Fiji (ImageJ, National Institutes of Health) (Schindelin et al., 2012) was used for image processing. Still images of time-lapse experiments are presented as z stacks at maximum intensity. Kymographs were generated using Fiji imaging software. Briefly, the stack of interest was aligned using StackReg plugin. Then a montage consisting of the different time-points was done from a horizontal rectangle of 5 μm located along the cell cortex.

For DIC and conventional fluorescence microscopy images (as shown in Figures 2A, 2B, 4A, 4E, 5A, 5C, 5E, 6A, 6C, S2, S4B, S5, and S6) we used a Nikon Eclipse 90i microscope equipped with differential interference contrast optics, a PLAN APO VC 100x 1.4 oil immersion objective, an ORCA-II-ERG camera (Hamamatsu) image acquisition software Metamorph 7.8.13 (Gataca Systems) and a LED illumination Cool LED pE-300lite. Fluorescence single plane images shown in Figure 2B were acquired on an inverted microscope (model IX71; Olympus) equipped with a PlanApo 100x/1.40 IX70 objective, a Personal DeltaVision system, a Solid State Illumination System InsightSSI™ Spectra7 (Applied Precision) a CoolSnap HQ2 monochrome camera (Photometrics) and softWoRx 5.5.0 imaging software (Applied Precision). Images were then corrected by 3-D deconvolution (conservative ratio, 10 iterations and medium noise filtering) using the softWoRx imaging software.

For cell length and cell width measurements, cells were stained with calcofluor (Sigma, F3543) and examined under the microscope.

Elongation rates assay using FITC

Novel growth zones were measured as described previously (Revilla-Guarinos et al., 2016). Briefly, yeast cells were grown to an OD_{600} of ~0.3. To minimize the effects of the media and other technical conditions, we co-cultured each mutant strain (lacking fluorescent markers) with the wild-type strain (expressing Hta1-mRFP) in MM containing 5 μg/ml of FITC-lectin (L9381, Sigma-Aldrich). After 15 min of incubation, cells were pelleted by mild centrifugation and washed twice with MM. Then cells were further incubated with pre-warmed stain-free media for 90 min. Finally, cells were counterstained with calcofluor white and observed under the microscope.

H_2O_2 sensitivity assay

To monitor cell growth upon stress imposition, growth curves were performed as described elsewhere (Calvo et al., 2009). Briefly, MM cultures at an initial OD_{600} of 0.1 were treated or not with the drugs and inoculated by duplicate in 96-well non-coated polystyrene microplates with an adhesive plate seal. Plates were incubated in a Power Wave microplate scanning spectrophotometer (Bio-Tek) at 30°C with continuous shaking. The OD_{600} was automatically recorded every 10 min for the indicated hours using Gen5 software.

TCA extracts and immuno blot analysis

Modified trichloroacetic acid (TCA) protocol was used for protein extraction as previously described (Jara et al., 2007). Briefly, TCA to a final concentration of 10% was added to *S. pombe* cultures at an OD_{600} of 0.5. Cells were pelleted and washed in 20% TCA. The pellets were resuspended in 100 μl of 12.5% TCA and lysed by vortexing in presence of glass beads. Cell lysates were pelleted, washed in acetone and dried. Pellets were resuspended in a Tris buffer (0.1 M Tris-HCl pH 8.0, 1 mM EDTA, 1% SDS), loading buffer was added and samples were boiled for 5 min at 100°C. Samples were separated by SDS-PAGE and detected by immunoblotting with polyclonal anti-Atf1 (Sansó et al., 2008), house-made monoclonal anti-HA antiserum (12CA5), polyclonal anti-Sty1 (Jara et al., 2007), monoclonal anti-GFP (Takara) and monoclonal anti-tubulin (T5168, Sigma-Aldrich) antibodies.

Protein production in *E. coli*

To produce and purify GST-tagged proteins, the protease deficient *E. coli* strain FB810 was transformed with the corresponding plasmids. A liquid culture of 200 ml was grown up to OD_{595} of 0.6, then 100 μM of IPTG was added to the culture and further incubated during 20 h at 18°C. Cells were collected and resuspended in STET buffer (50 mM Tris HCl pH 8.0, 1 mM EDTA, 150 mM NaCl, 5% Triton X-100, 1 mM DTT). Cell lysis was obtained by 5 pulses of sonication of 15 s at 40% amplitude. Soluble fraction was prepared by centrifugation at 10,000 rpm for 10 min at 4°C. A volume of 2.5 ml of soluble fraction was incubated with 100 μl of Glutathione

Sepharose beads (GE Healthcare, 17-0756-01) for 1 h at 4°C. Beads were washed three times with NET-N buffer (20 mM Tris-HCl pH 8.0, 1 mM EDTA, 100 mM NaCl, 0.5% NP-40). A final washing in Elution Buffer (100 mM Tris-HCl pH 8.0, 120 mM NaCl) was performed. Finally, the desired protein was eluted form the beads by incubation with 100 μl of Elution Buffer containing 6 mg/ml of GSH (Sigma, 4251) during 30 min at 4°C. Recombinant proteins were checked and quantified in a polyacrylamide gel and stained with Coomassie Brilliant Blue (Amresco, 0472). Purified proteins were stored at −80°C.

In vitro kinase assay

To perform kinase assays, two sequential enzymatic reactions were prepared. First of all, recombinant GST-Sty1 kinase should be activated by pre-incubation with its MAP kinase kinase, GST-Wis1.DD. To prepare reaction A, 0.2 μg of either GST-Sty1 or GST-Sty1.K49R was mixed with 0.02 μg of GST-Wis1.DD in 1x Kinase buffer (50 mM Tris-HCl pH 7.5, 50 mM KCl, 10 mM MgCl2, 1 mM DTT) containing 0.5 mM of freshly added ATP (Promega, E6011) in 10 μl reactions. Reaction A was incubated at 30°C for 5 min. Then it was mixed with an equal volume of reaction B containing 2 μg of the GST-substrate in 1x Kinase buffer and 2 μCi γ-^{32}P-ATP (PerkinElmer, BLU002Z250UC). The mix was further incubated at 30°C for 20 min. The enzymatic reaction was stopped by adding SDS-PAGE sample buffer. Proteins were boiled and separated into a polyacrylamide gel. Gels were dried overnight and the signal of γ-^{32}P-ATP was detected on an autoradiogram.

Protein sequence analysis

Protein domains as in Figure S8B and S9C were obtained using a simple modular architecture research tool (SMART) (http://SMART.embl-heidelberg.de). Canonical S/T-P phosphorylation sites were mapped manually.

QUANTIFICATION AND STATISTICAL ANALYSIS

Unless otherwise stated, all experiments were performed at least three times and representative experiments were shown. Several approaches were used for quantification of microscopy images.

To quantify Cdc42 depolarization from time-lapse experiments (as in Figure 1B, 3B, S3A, S3D, and S3F), the mean value of each cell cytoplasm was subtracted from the image in order to obtain pure CRIB signal at tips. Tip signal was narrowly selected using the square tool of Fiji software and integrated density of each tip was measured along the different time points. To obtain CRIB signal per cell, the values of both tips were added and the percentage of CRIB intensity was calculated by referencing all the values to the time zero.

For quantification of CRIB intensity at cell tips (as shown in Figure 4C, 5F, 6D, 6E, and S5D) we obtained the intensity profile from a 5-pixel wide line along the x axis of the cell. The two peak values, corresponding to the maximum pixel value of each tip, were added obtaining CRIB intensity per cell. For line-scans quantification (as shown in Figure 5B) a 5-pixel line was drawn along the cell tip and profiles for the GFP and mCherry channels were obtained. For the untreated cells Rga3-GFP profiles were centered to the maximum value of CRIB-3mCherry. In the case of peroxide treated cells, profiles were centered on the maximum value of the GFP channel.

For cell length and cell width measurements (as shown in Figure 4B, 4F, 6B, S4A, and S6B) only septated cells were analyzed. All cell measurements were performed manually using the line tool from Fiji software.

Elongation rates (as in Figure 4D) were calculated by dividing the novel length by the incubation time.

Graphs and statistical analysis were performed with either Prism (GraphPad Software) or the R package Ggplot2. Details of the statistical test used in each case can be found in the figure legend.